Chapter 21

Acoustic Wave Based Microfluidics and Lab-on-a-Chip

J. K. Luo, Y. Q. Fu and W. I. Milne

Additional information is available at the end of the chapter

http://dx.doi.org/10.5772/56387

1. Introduction

Microfluidics refers to a set of technologies that control the flow of minute amounts of liquids, typically from a few picolitres (*pl*s) to a few microlitres (μls) in a miniaturized system [1,2]. Lab-on-a-chip (LOC) systems typically consist of a set of microfluidics and sensors with dimensions from a few square millimetres (mm^2) to a few square centimetres (cm^2). Microfluidics handles liquids through droplet generation, transportation and mixing of liquid samples, chemical reactions etc. Sensors may include biochemical sensors, gas sensors and physical sensors such as humidity and temperature sensors, flow meter and viscometers etc. Therefore, LOCs are microsystems with a much broader meaning, and generally perform single or multiple laboratory processes and functions on a chip-scale.

Microfluidic and LOC systems have distinctive advantages:

- Low volume fluidic consumption (low reagents costs and less required sample volumes for analysis and diagnostics, less waste);
- Fast analysis and short response times due to short diffusion distances, high surface to volume ratios, small thermal capacity and fast heating rate;
- Better process control because of a faster response of the systems (e.g. thermal control for exothermic chemical reactions);
- Compactness of the systems owing to integration of many functionalities and the small dimensions of each component;
- Massive parallelization due to compactness, which allows high-throughput analysis;
- Low fabrication costs, allowing cost-effective disposable chips fabricated in mass production;
- Safe platform for chemical, radioactive or biological studies because of integration of functionality within the small systems and often on-board power generator.

Owing to their outstanding properties and great potential applications, microfluidics and LOCs have received tremendous interests from engineering, healthcare, medical research, drug-development sectors. They are regarded as the technologies of the future for great value-added manufacturing. So far, most of the LOCs and microfluidics are single function systems, the trend and demands are to develop LOCs and microfluidics with multi-functions.

Microfluidics and LOC systems based on acoustic waves generated through the piezoelectric effect have recently received a great attention, as acoustic waves can be utilized not only for actuation/microfluidics, but also for sensing/detection, allowing integration of various acoustic devices for LOCs to perform multi-functions. In this chapter, we will thus focus on the acoustic wave-based LOC systems.

1.1. Acoustic wave based microfluidics

Many microfluidic technologies have been explored and developed [1,3], including two major classes of devices: active devices such as micropumps, micromixers and droplet generators, and passive components such as microchannels, valves and microchambers. The mechanisms of micropumps vary widely. Based on the mechanisms, designs and applications, micropumps can be categorized into two main groups: mechanical and kinetic pumps. Mechanical micropumps typically represent miniaturized version of macro-sized pumps that typically consist of a microchamber, check valves, microchannels and an active diaphragm to induce displacements for liquid transportation. Thermal bimorph, piezoelectric, electrostatic, magnetic forces and shape memory mechanisms have been utilized to actuate the diaphragm in an oscillation mode [2,3]. These mechanical micropumps are complicated, expensive, typically made by multi-wafer processes, and are therefore difficult to be integrated with other microsystems such as integrated circuits (IC) for control and signal processing due to incompatible processes and structures [1,2,4]. They generally have a large dead volume, leading to an excessive waste of biosamples and reagents which are normally expensive and precious in biological analysis, especially for forensic investigations. These micropumps typically have moving parts (diaphragm and check-valves) which lead to low production yields in fabrication, high failure rates and poor reliability in operation.

The new trend is to develop non-mechanical or moving-part-free micropumps by utilizing electrokinetic forces and surface tension (or surface energy-related forces) such as the electroosmotic (EO) effect [5], electrophoresis (EP) [6], dielectrophoresis (DEP) [7,8], asymmetric electric field, electrowetting-on-dielectrics (EWOD) [9,10], electrostatic pumps [11,12] etc. Electrokinetic force based micropumps typically require electric/magnetic fields to mobilize ionic, or polarisable particles and species in a liquid which can drag the liquid through friction forces to form a continuous flow. The surface tension-based micropumps are typically droplet-based systems, which manipulate discrete droplets through modification of surface tension/energy by external stimuli [13]. Electric field, thermal and concentration gradients generated by localized heating or optical beams, photosensitization and capillary forces are used for these micropumps. Their key characteristic is that they can transport discrete droplets, acting as the so-called digital micropumps, on channel-less (or

wall-less) planar surfaces without check valves [13]. The fabrication process is simple and requires no special substrate. Therefore, these pumps can be easily integrated with electronics for control and signal processing etc.

Acoustic waves utilized in microfluidics and lab-on-a-chip systems include ultrasound, bulk acoustic waves and surface acoustic waves (SAW). Ultrasound generated by external large piezoelectric (PE) transducers has been widely utilized for microfluidics which is very effective in mixing microfluidics, and has recently been utilized for transportation of liquid [14] and particle sorting etc through novel design of the systems [15,16]. Due to the different mechanism, ultrasonic wave based microfluidics and LOCs will not be discussed here.

SAW-based microfluidics and LOCs are one of the latest technologies. SAW can be used as an actuation force for pumping and mixing liquids, and for generating droplets and mist [17, 42,18,19]. SAW micropumps can not only manipulate discrete liquid droplets from *pl*s to a few tens of μ*l*s, but can also pump a continuous fluid. SAW devices are also excellent sensors for monitoring physical parameters and detecting biochemical entities with high sensitivity. Furthermore the development of thin film SAW technology has opened the way for integration of SAW-based microfluidics and sensors with Si-based electronics on the same chip for LOCs with better functions and applications [20]. This chapter will mainly focus on acoustic wave technologies for microfluidics and lab-on-a-chip applications.

1.2. Acoustic wave resonant sensors

Sensors are a type of transducer that convert some physical stimulation such as temperature, pressure etc into electronic, optical, magnetic, or acoustic signals for quantitative measurement, while biosensors are devices that convert biological information into measurable electronic signals. Various technologies such as optical sensors, electrochemical sensors, field effect transistor based sensors, microcantilevers and acoustic resonators have been developed for sensing, particularly for biochemical sensing.

Compared with other biosensing technologies, acoustic wave based technologies have several advantages including simple operation, high sensitivity, small size, fast response and low cost, [21]. Another distinctive advantage of acoustic wave sensors over others is that they can be simply integrated with acoustic wave based microfluidics to form a LOC system driven by a single mechanism, which makes the system fabrication and operation much simpler.

There are four types of acoustic wave resonators: the quartz crystal microbalance (QCM), surface acoustic wave device (SAW), film bulk acoustic resonator (FBAR or BAW) and flexural plate wave (FPW) resonator. Acoustic wave sensors are able to detect not only mass/density changes, but also viscosity, elastic modulus, conductivity and dielectric properties. They have many applications in monitoring of pressure, moisture, temperature, force, acceleration, shock, viscosity, flow, pH levels, ionic contaminants, odour, radiation and electric fields [22,23]. By using specific gas absorbents and biological markers, the acoustic resonators can be made into gas sensors and biosensors. As the latter is the main focus of this chapter, we will only discuss acoustic wave biosensors here.

QCMs with a structure shown in Fig. 1 have a long history, and probably are the only one currently being commercialized and practically used. By cutting a quartz crystal with proper orientations, it is possible to make QCM sensors operate in a longitudinal mode as well as in a transverse (also called thickness shear) mode. The standing waves in the thickness shear-mode devices are parallel to the surface of the QCM plate, and the wave energy is largely preserved in the presence of liquids, therefore the shear mode QCM is suitable for sensing in liquid environments, a pre-request and necessary condition for most biosensing and physiological monitoring. QCM sensors have the advantages of simplicity in design and operation and a mature technology.

Figure 1. Typical QCM resonator.

The sensitivity of acoustic wave resonators is determined by the square of the resonant frequency, f_r, and base mass. The frequency shift Δf of an acoustic wave resonator induced by a mass loading, Δm, is described by [24]

$$\Delta f = \frac{2\Delta m f_r^2}{A\sqrt{\rho\mu}} \tag{1}$$

where A, ρ, μ and f_r are the area, density, shear modulus and intrinsic resonant frequency (sometimes defined as the operating frequency, f_0), respectively. QCM sensors have a fundamental limitation of low sensitivity due to the thickness of wafer and the large active area, hence low f_0 and large base mass.

SAW sensors consist of a pair of interdigitated transducers (IDTs) (Fig. 2). When a series of radio frequency (R.F.) signals are applied to one of the IDTs, surface acoustic waves are generated through the piezoelectric effect, and travel along the surface of the substrates, received by the IDT on opposite. The strength of the waves decays exponentially with depth into the substrate. Depending on the nature of the travelling acoustic waves, SAW can be longitudinal or transverse mode. The operating frequencies of SAW devices are typically in the range of 100-300 MHz, and the active base mass is much smaller than that of QCMs owing to the one wavelength depth of active area. Therefore, the sensitivity of SAW sensors could be much higher than that of the QCMs. The acoustic waves of shear mode SAW devices travel parallel to the surface with no longitudinal component with no acoustic energy dissipated into the liquid in contact. Therefore, the shear mode SAW devices are suitable for sensing in liquids. Furthermore rapid advances in thin film deposition technologies allow fabrication of

high quality thin film SAW devices, resulting in the possibility for integration of SAW sensors with electronics on the same chip. Advantages of the SAW sensors are: simplicity in device structure and process, high sensitivity, small size compared to QCM, availability of thin film SAW, and the possibility for integration of SAW sensors with Si-electronics. However similar to QCM, the SAW devices are difficult to scale down, and other concerns include weak signal, relatively low quality factor and relatively low sensitivity.

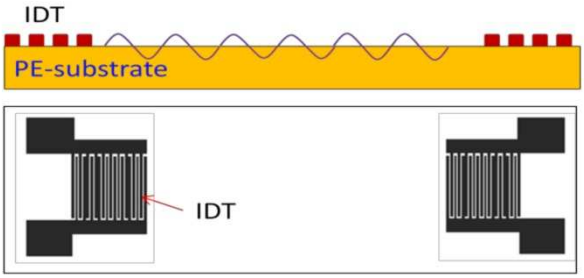

Figure 2. Typical structure of a SAW resonator.

FBARs are newly emerging acoustic nanodevices [25,26,27], with a structure similar to that of QCM as shown in Fig. 3, but thousand times smaller with a typical size from 100 μm × 100 μm to 30 μm × 30 μm and a thickness of a few micrometers. The operating frequency of FBARs is in the range from sub-gigahertz to a few GHz. The base mass of a FBAR is much smaller than those of the QCM and SAW devices owing to the much reduced area and thickness, and the sensitivity of FBAR sensors can be dramatically increased compared with other acoustic sensors as shown in Fig. 4 [28]. FBARs have the highest sensitivity, and the SAW devices are in the middle with the QCM ones the lowest.

FBARs have three basic structures: the Bragg acoustic mirror type (Fig. 3a), the back-trench type (Fig. 3b), and the air-bag type (Fig. 3c&3d). The Bragg reflector based FBARs are normally made on PE-films deposited on a solid substrate. The acoustic mirror is composed of many quarter-wavelength layers with alternating high and low acoustic impedances. Due to the high acoustic impedance ratio of the acoustic mirror, the acoustic energy is reflected and confined within the top piezoelectric layer, thus maintaining an excellent resonant bandwidth even on a solid substrate. This structure has a better mechanical robustness and a simpler fabrication process. Also cheap substrates such as glass or plastics may be used for the FBAR fabrication to reduce the cost [29]. The shortages of the Bragg reflector FBARs are long film deposition process and the difficulty in precise control of the layers thickness which may lead to poor quality factor. The back trench mode FBARs are typically made on a thin membrane with a thickness about 1-2 μm to reduce the base mass and increase the robustness. The back trenches are made either by anisotropic wet etching or by deep reactive ion etch (DRIE). The air bag types of FBARs are another type of back-trench type of FBARs, but with the large back-trench replaced by a small gaps formed through etching processes to remove the supporting material underneath. It has either a “standing-out” structure formed by a thin sacrificial layer or a “digging-in” structure.

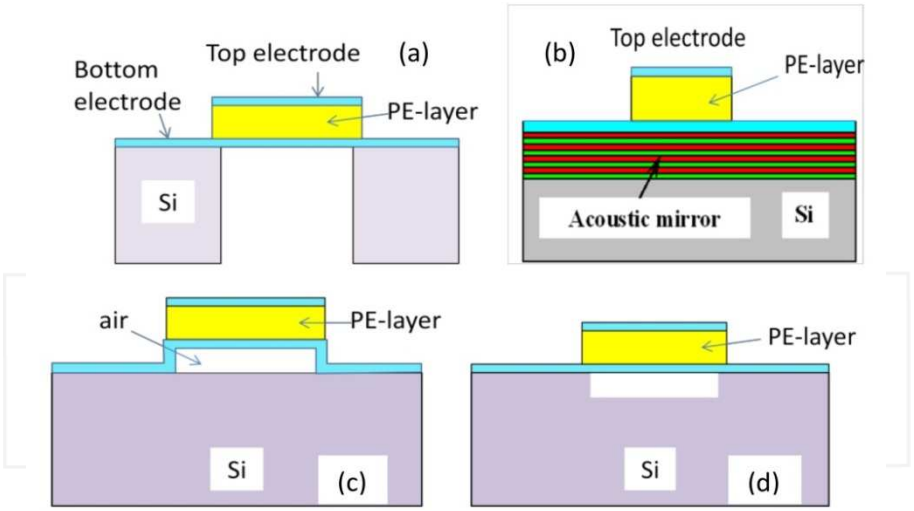

Figure 3. Various structures of FBARs. a) Back trench mode, b). Bragg reflector mode, c). Standing-out air bag mode and d). Digging-in air bag mode.

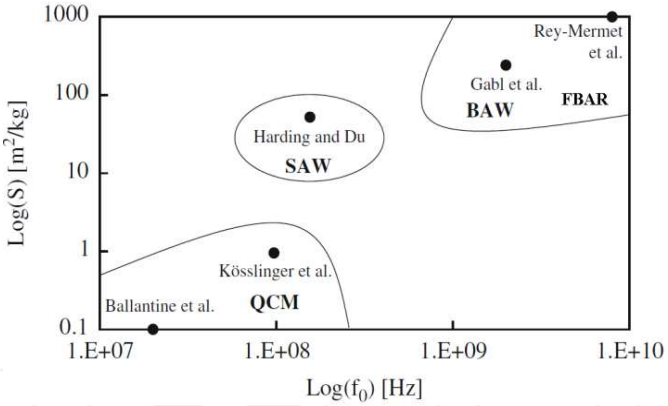

Figure 4. Comparison of sensitivity of QCM, SAW and FBAR biosensors. FBAR resonators have the highest sensitivity owing to its much reduced base mass and high operating frequency [28]. Reprinted with permission from Elsevier, Sensors and Actutars, B 114, 2006, 681.

FBARs also have extremely small size which allows the use of an array of FBARs for multiple-sensing in parallel. Also because they are based on thin film technology, the FBARs can be simply integrated with other acoustic microfluidics, microsystems and Si-electronics for LOC applications. Thickness shear mode FBARs have been tried by using off c-axis crystal materials with some success [30,31]. It is still not a simple task to obtain c-axis inclined film materials for low cost FBARs.

In a manner similar to a SAW device, flexural plate wave resonators (also called Lamb wave, and often regarded as the ultrasonic wave [32,33]) (Fig. 5) on a membrane have been

developed for biochemical sensing in liquid [34]. The Lamb wave velocity in the FPW resonator is much smaller than that of the acoustic waves, and the dissipation of wave energy into the liquid is minimized, therefore it can be used for liquid sensing directly. The sensing mechanism is based on the detection of a relative change in wave magnitude induced by the perturbation on the membrane, rather than the resonant frequency shift as they would be very small. The sensitivity of the FPW devices increases as the membrane thickness becomes thinner [35,36]. The main drawback of the FPW biosensors is that there is a practical limit on the minimum film thickness due to the fragility. Compared with the other three types of acoustic wave sensors, FPW devices as sensors still need much further development.

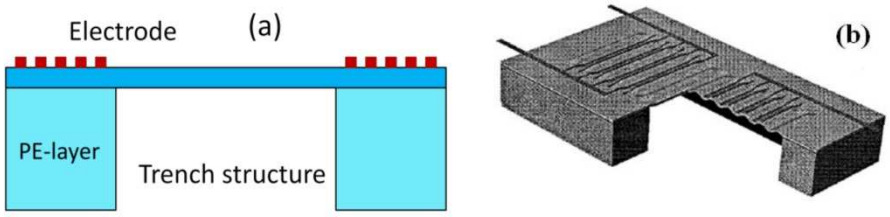

Figure 5. Typical structure of a flexural plate wave resonator.

1.3. Piezoelectric thin film technologies

QCM and SAW devices are typically fabricated using bulk materials which are expensive and cannot be integrated with electronics, microfluidics and sensors on the same substrate for applications. Various thin film-based QCMs [37,38], SAW devices [39,40,41] and FBARs [25,26,27] have been developed. PZT, ZnO and AlN piezoelectric thin films have good piezoelectric properties and high electro-mechanical coupling coefficient, k^2, thus they have been studied intensively for this purpose. They can be grown in thin film form on a variety of substrates such as Si, making these materials very promising for integration with electronic circuitry, particularly for devices aimed at low-cost and mass production for one-time use. PZT has the highest piezoelectric constant and k^2, but PZT films have very high acoustic attenuation, lower sound wave velocities, poor biocompatibility and worst of all, the requirement for extremely high temperature sintering and high electric field poling, making them unsuitable for integration with electronics. AlN and ZnO are the most common thin films used for SAW, FBARs and FPW devices. AlN is chemically inert and stable, with high acoustic velocity, but AlN thin films are relatively difficult to deposit, requiring stringent optimization for the process to obtain high quality thin films with smooth surfaces and right crystal orientations. On the other hand, ZnO PE films with a high PE quality are much easier to obtain using various deposition technologies such as sputtering, laser-ablation, chemical vapour deposition (CVD) and molecular beam epitaxy (MBE) etc, therefore, it is the most widely used PE material for thin film acoustic wave devices. The acoustic velocity of ZnO thin films is about 2700 m/s, smaller than that of AlN (11050 and 6090 m/s for longitudinal and transverse modes, respectively); hence ZnO SAW has a lower operating frequency than that of

the AlN SAW devices. For wider applications, high operating frequency ZnO SAW devices have been developed by using non-PE supporting layers with high acoustic velocity such as sapphire and diamond [39, 40, 41]. Acoustic waves generated by ZnO SAW travel inside the supporting layer with high velocity, resulting in higher frequencies. Besides PZT, AlN, and ZnO, many other PE thin films have been developed, mostly for SAW device applications. Gallium arsenide, gallium nitrides, polyvinylidene fluoride (PVDF) and its copolymers are a few that have been investigated for piezoelectric applications.

2. Modelling of surface acoustic wave microfluidics

Microscale mixing and pumping are essential processes for microfluidic and LOC applications for biochemical analysis, disease diagnosis, DNA sequencing and drug development etc [42,43]. Various technologies have been developed. SAW based microfluidics is one of the most advanced technologies, which utilize SAW induced forces for pumping, mixing, droplet generating and ejecting etc. In this section, the interaction between the SAW and liquid is theoretically analysed, to show that the complicated acoustic streaming and particle sorting etc are physical phenomena which can be well addressed by theoretical model.

2.1. Navier-Stoke equation for fluid motion

It is well known that radiation of a high-intensity beam of acoustic waves into a liquid can result in acoustic streaming. Absorption of the acoustic energy results in significant attenuation of acoustic energy and moment in the fluid within a short range, meanwhile consumption of the energy leads to fluid motion. This phenomenon was observed by Lord Rayleigh in 1884 [44] and was then further studied in detail by Westervelt in 1951 [45] and Nyborg [46] in the 1960s'.

Under an external body force, F_j, induced by acoustic waves, the fundamental hydrodynamics of a steady viscous fluid is governed by Navier-stoke equation [47],

$$(V_i.\nabla)V_j = F_j - \frac{1}{\rho}\nabla p + \eta\nabla^2 V_j \tag{2}$$

where V is the acoustic streaming velocity (or the particle velocity), p the pressure, ρ and η are the fluid density and shear viscosity coefficient, respectively. It is generally assumed that the fluid flow exhibits viscous and incompressible laminar flow. Here the subscripts i and j = 1, 2, 3 represent the x, y and z coordinates respectively for a 3-dimentional (3D) phenomenon. The nonlinear body force is correlated to the Reynolds' stress, σ, induced by the acoustic wave in the fluid with spatial variation in all three coordinates [46],

$$\sigma_{ij} = \rho\overline{v_i v_j} \tag{3}$$

where v_i and v_j are the velocity fluctuations in x, y and z directions. The stress is a mean velocity fluctuation and density product represented by the upper bar. The relation for the force and the Reynold's stress is expressed as,

$$F_j = -\sum_{i=1}^{3} \frac{\partial \overline{v_i v_j}}{\partial x_i} \tag{4}$$

According to the continuity equation, the following equation applies,

$$\frac{\partial \rho}{\partial t} + \nabla . \rho \mathrm{V} = 0 \tag{5}$$

For a steady flow, the first term is zero and we obtain,

$$\nabla . \rho V = 0$$

This leads to zero for the right side of eq.(2),

$$F_j - \frac{1}{\rho} \nabla p + \eta \nabla^2 V_j = 0 \tag{6}$$

The governing equation of the acoustic streaming force has been derived by Nyborg [46] for an incompressible fluid, and is given by the following equation;

$$-F_j = < V_{aj} . \nabla V_{aj} > + V_{aj} < \nabla . V_{aj} > \tag{7}$$

where V_a represents the acoustic wave velocity (different from the streaming velocity V), and the brackets < > indicate the time averaged value [46,48]. Therefore, the nonlinear acoustic streaming force F_j can be calculated, once the wave velocity is known.

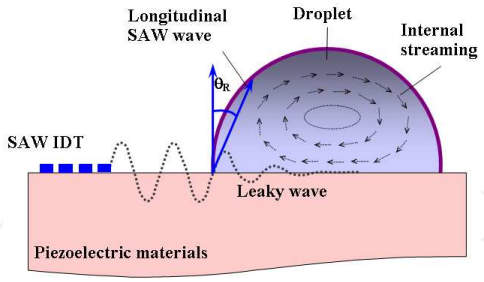

Figure 6. Schematic drawing of acoustic streaming in liquid fluid induced by SAW. The direction of SAW induced streaming is determined by the Rayleigh angle.

Acoustic waves travel in a solid medium with a relatively small attenuation. The attenuation becomes large once the waves enter the fluid medium and decays exponentially. Therefore the acoustic wave generated force is a short range force. Figure 6 schematically shows SAW induced acoustic streaming in a droplet.

The SAW travelling along the surface of the PE substrate has a small surface displacements typically less than one nanometre. The SAW changes its mode into a leaky SAW once it interacts with any liquid medium in its path. This leaky longitudinal SAW continuously

travels within the liquid medium with the streaming angle determined by the Rayleigh angle Θ_R [49,50,51], as depicted in Fig. 6 according to the following equation;

$$\theta_R = \sin^{-1}\frac{V_L}{V_S} \tag{8}$$

where V_S is the Rayleigh SAW velocity on the piezoelectric substrate, and V_L is the acoustic velocity in the liquid. The leaky SAW has been well studied, and the displacement, (u_x, u_y), of the acoustic wave in the liquid is sinusoid in form with an exponential decay with distance. For a 2D case, the displacement can be expressed by [52],

$$u(x,t) = A\exp(-l(x)/l_S)\sin(\omega t - k.x + \varphi) \tag{9}$$

where A is equivalent to the SAW amplitude at the point of entry into the liquid, $\omega = 2\pi f$, the angular frequency imposed by the SAW, l(x) is the path length along the wave path, and $\boldsymbol{k}$ is the wave vector of the acoustic wave. Streaming is a 3D phenomenon, especially for streaming inside a droplet; therefore displacements in all directions have to be considered. The displacements in the x and y directions are expressed by [47,53];

$$u_x = A\exp.(j\omega t).\exp(-jk_L x).\exp(-\alpha k_L y) \tag{10}$$

$$u_y = -j\alpha A\exp.(j\omega t).\exp(-jk_L x).\exp(-\alpha k_L y) \tag{11}$$

Here, α represents the attenuation constant;

$$\alpha^2 = 1-(\frac{V_S}{V_L})^2 \tag{12}$$

where V_S and V_L are the leaky (Rayleigh) SAW velocity and the sound velocity in liquid respectively. $K_r=2\pi/\lambda$ is a real number, where λ is the wave length and the leaky SAW wave number ($k_L=k_r+jk_i$) is complex with the imaginary part, jk_i, representing the SAW energy dissipation within the liquid. The leaky SAW wave number can be obtained by extending the method of Campbell and Jones [54, 47] into the solid-liquid structure assuming both stress and displacement to be continuous at y=0, and V_L=1500 m/s for water (Most of the biofluid is water-based, V_L changes if other liquid is used.). If the wave displacements (u_x, u_y) are replaced by the wave velocities using $V_j = \frac{\partial u_j}{\partial t}$ and substituting into eq.(7), the two components of streaming force can be obtained for an incompressible fluid as follows [47,53];

$$F_x = -(1+\alpha_1^2)A^2\omega^2 k_i \exp 2(k_i x + \alpha_1 k_i y) \tag{13}$$

$$F_y = -(1+\alpha_1^2)A^2\omega^2 k_i \alpha_1 \exp 2(k_i x + \alpha_1 k_i y) \tag{14}$$

where, $\alpha = j\alpha_1$. The total SAW streaming force F can be calculated by $F = \sqrt{F_x^2 + F_y^2}$, which is then given by;

$$F = -(1+\alpha_1^2)^{\frac{3}{2}} A^2 \omega^2 k_i \exp 2(k_i x + \alpha_1 k_i y) \quad (15)$$

The SAW force F acts on the main fluid volume as a body force, but the exponential decay of the leaky SAW limits the influence of this force within the whole fluid within the decay distance. This leads to a complete diminishing of the acoustic force within a few hundreds of micrometers from the interaction point between the SAW and the liquid.

The numerical simulation of acoustic streaming is a complicated process and should be treated case by case due to the different designs of the systems. One must solve the full set of nonlinear hydrodynamic equations consisting of the Navier-Stokes equations, the continuity equation and an equation of state for an incompressible fluid driven by the time-dependent boundary condition. The majority of researchers have implemented the modelling by using existing software such as COMSOL or ANSYS. The numerical simulation requires a few software modules to implement the multiphysics modelling for the solid components as well as the viscous liquid body, and requires the consideration of coupling between the modules. For the viscous liquid, a Finite Volume Method (FVM), OpenFOAM-1.6 CFD code (OpenCFD LTD) and Surface Evolver are often used [55, 53,].

2.2 Modelling of acoustic streaming induced by SAW

The interaction of SAW with liquid depends on the position of the SAW relative to the liquid. Figures 7a&7b show two cases of the interaction of a SAW with a droplet: (1) the droplet is in the path of surface acoustic wave with droplet size smaller than the aperture of the IDT of the SAW device; and (2) the droplet is partially on the SAW path.

The interaction of the SAW with the liquid is a dynamic process involving a transition of the flow. Figure 8 shows a comparison of the transitional and steady streaming velocities induced by a leaky SAW obtained numerically and experimentally with RF power as a function [53]. As can be seen, the streaming velocity increases with time rapidly, and becomes stable after the transitional period. The transition time is in the range up to a few hundreds of milliseconds, depending on the RF power applied.

The streaming pattern depends on the entry angle of the SAW into the liquid. Figure 9 demonstrates the different streaming patterns generated by a SAW entering from the centre

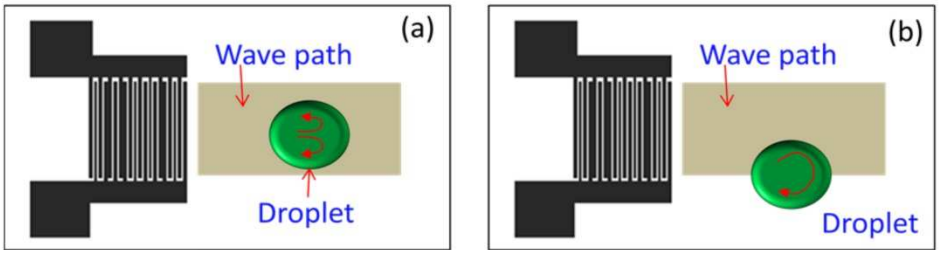

Figure 7. (a) Illustration of a droplet positioning symmetrically on surface of a SAW device; (b) asymmetric positioning of water droplet on the SAW device.

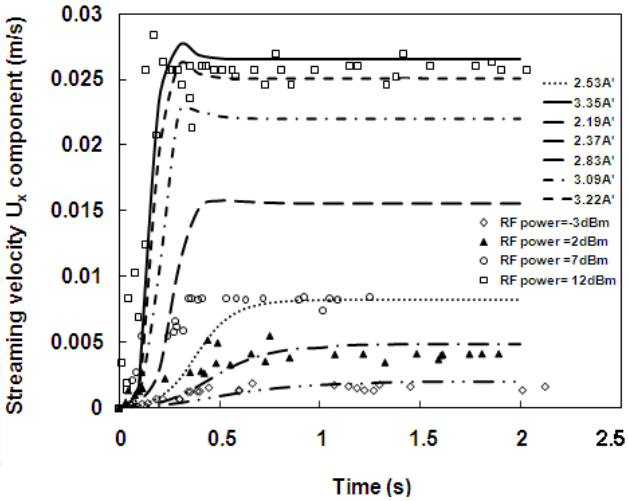

Figure 8. Streaming velocity at top centre of a 30μl droplet. SAW device has f=62MHz, an aperture of 2mm; Solid lines represent numerical results at different wave amplitudes; the symbols are experimentally measured data at different RF powers [53]. Reprinted with permission from Institute of Physics, J. Microeng. Micromech. 21, 2011, 015005.

and edge of the droplet [52]. A SAW entering in the centre of the droplet results in a symmetric shaped streaming pattern, with the highest velocity at the edge of the droplet where the SAW enters. When the SAW meets the droplet off-the central wave path, the streaming patterns is asymmetric and the degree of symmetry depends on the entry position of the SAW. A SAW entering into the droplet with a large off-centre line generates a large asymmetric flow pattern. As can be seen from Fig. 9, the numerical simulation can successfully reproduce the experimental results.

Modelling predicts that the streaming velocity is proportional to the RF power applied to the IDT electrode, in agreement with the experimental results, regardless as to whether 2D or 3D simulation was used. Figure 10 shows one of the results obtained by Alghane et al [53], demonstrating that the steady streaming velocity is approximately linearly correlated to the RF power applied.

For better understanding, 3D simulation is necessary to study the streaming phenomenon induced by leaky wave [44]. Figure 11 shows the simulated streamlines with a 3D circular flow pattern for a 30 μl droplet. The simulation results show that the highest value of a streaming velocity is located at the interaction area between the droplet and SAW as the highest momentum is delivered at this point. It attenuates rapidly as it enters the liquid droplet, in agreement with the experimental observation.

It is clear that the liquid initially moves at the Rayleigh angle before reaching the top of the droplet. It moves backward due to the constraint of the droplet boundary, forming a back flow on the two sides and the bottom of the droplet. Figure 12 is a comparison of the streaming patterns obtained experimentally and numerically, showing a good matching of

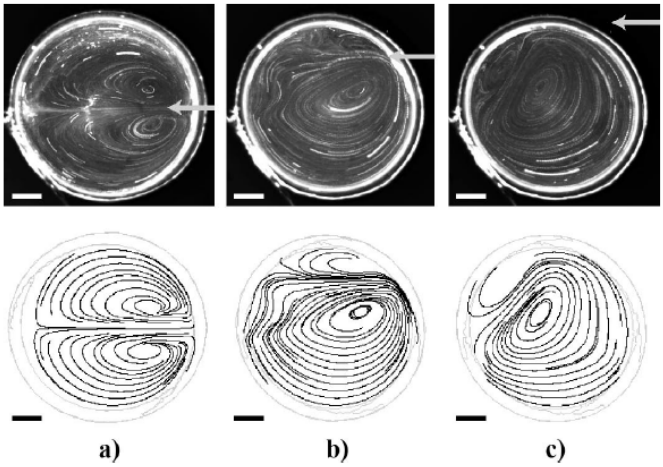

Figure 9. Comparison of streaming patterns for experiments and modelling. The narrow is SAW entering position from: (a) centre, (b) intermediate, and (c) outer part. The upper images are experimental results, while the bottom ones are the corresponding simulation results [52]. Reprinted with permission from IEEE, Transact. On Ultrasonics, Ferrelectrics and Freq. Control, 55, 2008, 2298. 1.

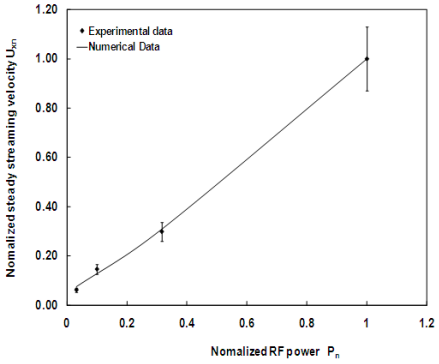

Figure 10. Flow normalized streaming velocity as a function of normalized RF power for a 30μl droplet size using a 128º YX-$LiNbO_3$ SAW device (IDT with 60 fingers) [53]. Reprinted with permission from Institute of Physics, J. Microeng. Micromech. 21, 2011, 015005.

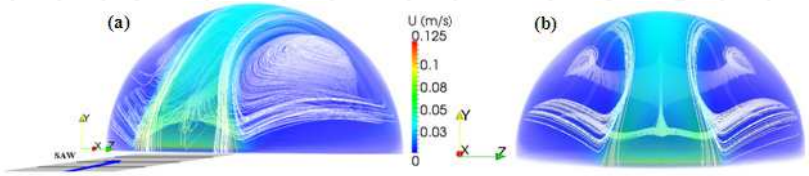

Figure 11. Acoustic streaming in 3D reproduced by numerical simulation in tilted view (a) and direct view (b). The droplet has a volume of 30ul, and the SAW enters through droplet centre [53]. Reprinted with permission from Institute of Physics, J. Microeng. Micromech. 21, 2011, 015005.

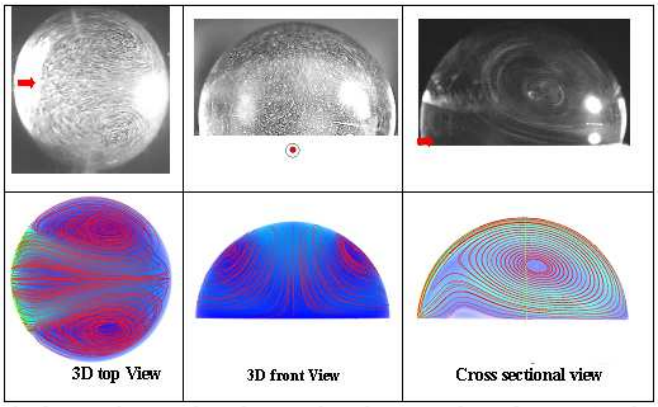

Figure 12. Comparison of experimental (upper row) and numerical modeling (bottom row) results for a 30μl droplet. SAW enters in a centre position of the droplet as shown by red arrow [53]. Reprinted with permission from Institute of Physics, J. Microeng. Micromech. 21, 2011, 015005.

the patterns. These numerical simulation results have clearly demonstrated that the chaotic acoustic streaming can be well explained by the physical laws.

3. Acoustic wave micropumps and micromixers

Although SAW devices have been commercialized over 60 years, applications in microfluidics and LOCs are only recent event. They are found to be very effective and efficient in microfluidics and LOCs [56]. SAW-based micropumps are one of them, and can transport liquid in a droplet form as well as in a continuous mode through proper design of a fluidic system. Acoustic streaming is also the most effective method of mixing liquids in small dimensions as it is quick and efficient, typically taking less than a few seconds to reach >95% mixing [57, 58]. In this section, SAW pumping and mixing are discussed.

3.1. IDT and SAW device structures

For microfluidics, one IDT electrode is enough for most pumping and mixing applications. The acoustic streaming velocity depends on the power output of the SAW devices and the amplitude of the RF signal applied to the IDT electrode. To obtain efficient acoustic streaming, it is desirable to have IDT electrodes with high and efficient power output. The SAW IDT design is important for delivering efficient SAW power output. The conventional bidirectional IDT may not be the most efficient for pumping and mixing, as the waves propagate in two opposite directions with half of the acoustic energy wasted. The simplest way is to reflect back some of the waves (Fig. 13a) by using reflector IDT. More sophisticated IDT designs include [59,60]: (a) split IDTs (Fig. 13b); (b) a SPUDT (single phase unidirectional transducer, Fig. 13c) which has the internally tuned reflectors within the IDT to form a unidirectional SAW propagation from one side of the IDT. These unidirectional acoustic wave transmission are essential for SAW microfluidics and sensors as they not only improve the performance, but maintain the SAW devices at the best operating conditions.

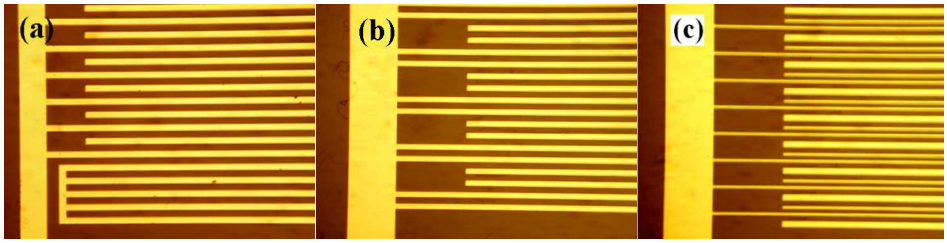

Figure 13. Common designs of IDT electrodes used for SAW devices. IDT with reflector (a), slitting electrode (b), and single phase unidirectional transducer (c).

Generally SAW IDT electrodes are so designed that the transmission spectra of the SAW devices have the highest quaility factor, Q, i.e. with a single well defined resonant peak with the highest amplitude. For microfluidic applications, the resonant frequency of a SAW device is changed slightly once liquid is loaded on the surface of the SAW device due to mass loading effect. It would be difficut to apply an RF signal with the exact frequency match to that of the SAW device, leading to the operation of SAW-microfluidics under mismatching conditions. This could be detrimental to the SAW devices as a much higher RF power is required to obtain the acoustic streaming effect, leading to overheating etc. Therefore a SAW device with a certain bandwidth of frequency would be better for SAW-microfluidic applications.

Thin film SAW devices have different transmission properties from those of SAW devices made on bulk substrates. Since the acoustic velocity of the thin film is different from that of the substrate, the acoustic waves generated by the top PE film layer may disperse into the substrate, i.e. some of waves propagate inside the substrate, resulting in two acoustic wave modes related to the PE layer and the substrate. A Sezawa mode acoustic wave is generated when the acoustic velocity in the substrate is higher than that in the PE-layer, and has been intensively studied as it can obtain SAW devices with high resonant frequencies using

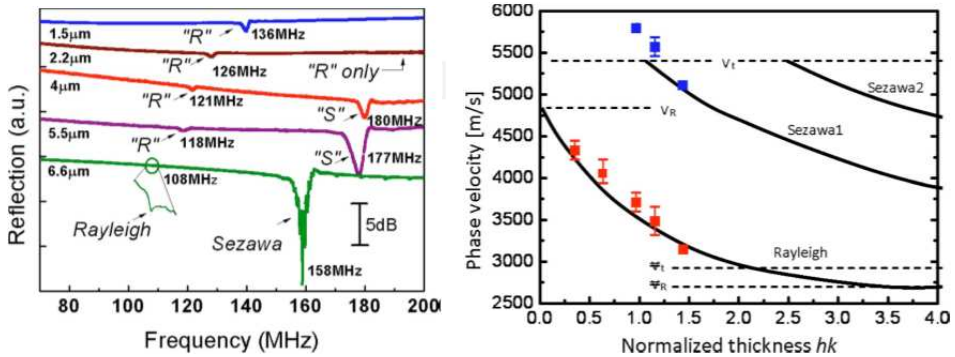

Figure 14. Reflection spectra of ZnO/Si SAWs with ZnO thickness as a parameter. The resonant frequencies of both Rayleigh and Sezawa waves decrease as the thickness increases, but the amplitudes of Sezawa waves are much larger than those of Rayleigh wave [61]. Reprinted with permission from AIP, Appl. Phys. Lett. 93, 2008, 094105.

conventional photolithography technology. Examples include ZnO films on Si, sapphire and diamond films. ZnO has a slow acoustic velocity of ~2700m/s, but ZnO SAW devices on a diamond layer can achieve a velocity over 10,000 m/s, close to those of the diamond substrate [39,40,41]. The acoustic velocity of the Sezawa waves depends on the thickness of the PE-layer, and can be well explained by the model of a layered structure. Figure 14 shows the dependence of the acoustic velocity of Rayleigh and Sezawa waves in ZnO/Si structures [61]. Sezawa waves often have much higher signal amplitude and resonant frequencies, particularly suitable for microfluidics and sensing applications.

3.2. SAW micropumps and micromixers

When the liquid is in the SAW path, acoustic moment and energy can be coupled into the liquid to induce acoustic streaming and flow. This has been utilized for fabrication of acoustic microfluidic systems, and many devices have been developed [62,63,64]. Generally speaking, both experimental and modelling results showed that acoustic waves can induce significant acoustic streaming in the liquid and result in mixing, pumping, ejection and atomization [65,66]. It was found that if the force is large enough, it can generate a significant acoustic streaming within the droplet (Fig. 15b). If the SAW device is immersed in a liquid container and an RF signal is applied to the IDT electrode, a steady flow pattern with a butterfly or quadrupolar streaming patterns can be obtained as shown in Fig. 15c. Significant acoustic streaming can facilitate internal agitation, which can speed up biochemical reactions, minimize non-specific bio-binding, and accelerate hybridization reactions in protein and DNA analysis which are commonly used in proteomics and genomics.

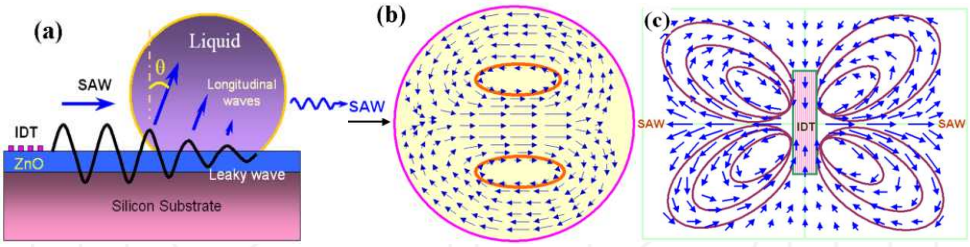

Figure 15. Patterns of acoustic streming in a droplet and in bulk liquid.

The SAW microfluidics have distinct advantages over other microfluidics, such as a simple device structure, no moving-parts, electronic control, high speed, programmability, manufacturability, remote control, compactness and high frequency response [67, 68,69]. The streaming velocity is proportional to the RF power applied, and could reach tens of centimetres per second. This is several orders of magnitude larger than other microfluidics, which are typically in the range of hundreds of micrometres to several millimetres per second [1,2,13]. Figure 16 shows the streaming velocity as a function of the amplitude of RF signal for LiNbO3 SAW devices with the IDT structure as a parameter [70]. It shows that the SAW device with a shorter wavelength has more power to induce streaming with higher velocity, and more IDT fingers are beneficial for coupling more RF power into the liquid. Du

et al. also demonstrated that the third harmonic resonant waves can also be used for acoustic streaming though the streaming velocity is reduced to a third of the fundamental mode wave induced streaming [70] as higher harmonic modes have much lower RF output.

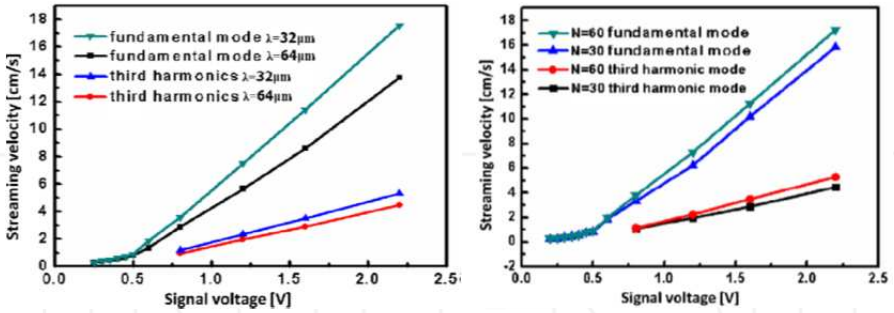

Figure 16. Acoustic streaming velocity as a function of RF signal voltage with finger pair and wave mode as parameters. [70]. Reprinted with permission from Institute of Physics, J. Microeng. Micromech. 19, 2009, 035016.

The streaming velocity depends on the RF power (or the signal voltage) applied to the IDT electrode. If the power is small enough and the droplet size is larger than the apperture of the IDT electrode, then the streaming velocity is proportional to the power as shown in Fig. 16, in agreement with the theoretical prediction as shown in Fig. 10. Once the power is over a certain range, velocity saturation is observed [71], and is believed that acoustic heating is responsible for the deviation from the linearity. Also the streaming velocity depends on the relative dimensions of the droplet and IDT aperture. At a fixed IDT aperture, a small doplet will have a low streaming velocity as the RF power can not be fully coupled into the liquid, and the streaming velocity increases with the droplet size, then reduces as the droplet size becomes larger than the aperture of the IDT. Therefore it is necessry to use an optimumal size/aperture ratio for a high performance SAW micromixer.

For streaming in a droplet, the boundary of the droplet becomes the boundary of the vortex, and the flow is confined within the droplet. This can be used for droplet-based mixing as shown in Fig. 17 by Xia et al on a $LiNbO_3$ SAW device [72]. Two drops with different contents are merged by a SAW, and immediate mixing occurs partially due to the kinetic energy involved and partially due to the acoustic streaming. This demonstrates the effective and efficient mixing of water and red dye droplets. The mixing process is completed in tens of ms, much shorter than those of most other micromixers.

Acoustic streaming has circulating flow patterns due to the back flow of the streaming as schematically shown in Fig.15 regardless as to whether it is a droplet or bulk liquid. This is caused by the short range of the acoustic force as discussed above. Directional flow by acoustic streaming, or liquid pumping, might be difficult due to this back flow. For pumping liquid in a specific direction, the SAW device and microchannels have to be arranged properly. Figure 18 is a schematic drawing of a SAW-based micropump. When the SAW-induced vortex size is smaller than the channel width, the SAW induces a circulating

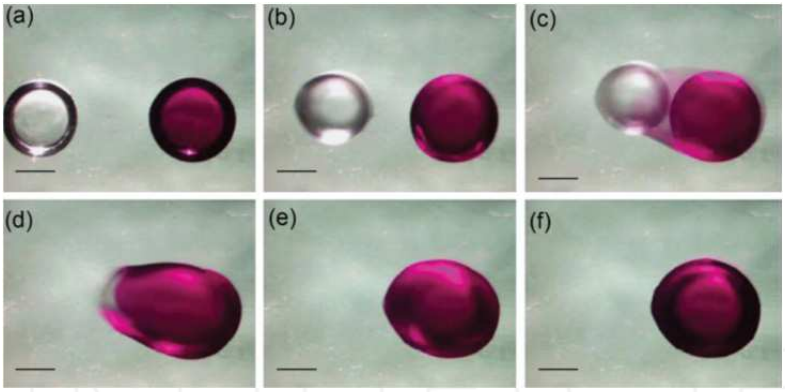

Figure 17. A water droplet and a red dye droplet mixture at (a) t=0s, (b) t = 4.066 s, (c) t = 4.4 s, (d) t = 4.466 s, (e) t = 5.000 s, and (f) t = 6.133 s [72]. Reprinted with permission from Elsevier, Talants, 84, 2011, 293.

vortex within the channel, and no net flow along the channel is produced. This can be utilized for in-channel mixing with high efficiency, but not pumping. When the size of vortex is larger than the width of the microchannel, the back flow is restricted by the channel wall, leading to a net directional flow along the channel. By using a channel with the width less than 200 μm, Yeo et al realized a SAW-based micropump [19].

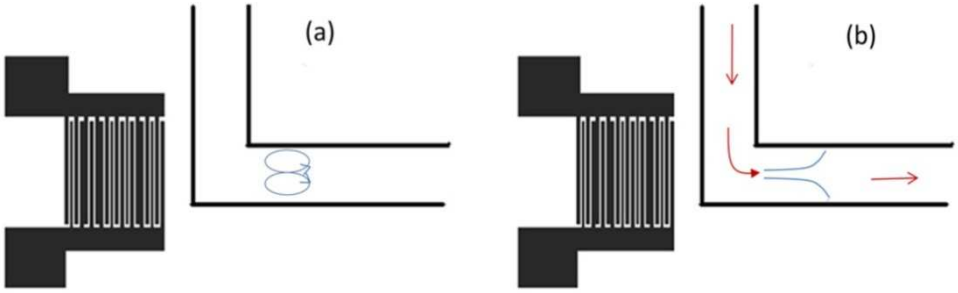

Figure 18. Principle of SAW-based micropumps with a channel. When the vortex is smaller than the channel width, the back flow occurs, suitable for in-channel mixing (a). When the vortex is larger than the channel width, a unidirectional flow is formed (b).

SAW has also been explored for in-channel mixing. Figure 19 shows two schemes used by Nguyen et al for in-channel mixing [73]. The microchannel is perpendicular to the SAW propagation direction. When a travelling acoustic wave encounters the liquid in the channel, streaming can be very effective mixing mechanism, and this mixing can be further enhanced by using curved IDT structures as shown in Fig. 19b. An alternative micromixing using SAW is to couple surface acoustic waves into liquids in a container to introduce agitation for mixing. As the streaming angle is determined by the Rayleigh angle, when a container is placed on a SAW device with a soft coupler on the surface, the SAW device can be an effective mixer [74].

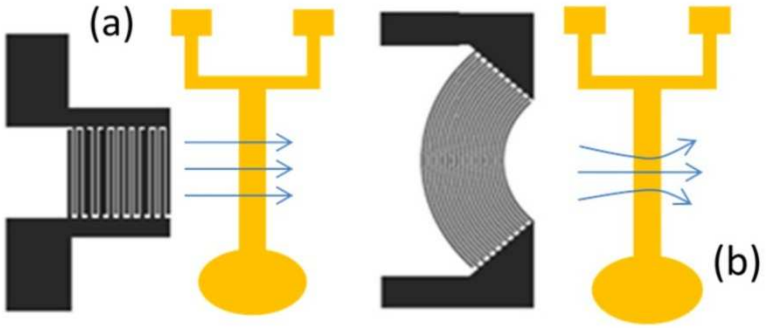

Figure 19. Schematic drawing of SAW-based in-channel micromixer.

SAW can be utilized for moving liquid droplets. If the liquid is on a hydrophobic surface with a contact angle larger than 90°, then the acoustic force may move the droplet along the wave path if the RF power is sufficiently large. Droplet-based microfluidics and LOCs are attractive as it provides the foundation for digital analysis and digital medicine with better and accurate results. The surface of most PE materials, however, is hydrophilic with water contact angle less than 90°. Surface acoustic waves are not strong enough to move the liquid on hydrophilic surfaces. Figure 20 shows the shape change of a droplet when it is subjected to an acoustic pressure on a hydrophilic surface. Water droplets cannot be moved freely on the surface under the stimulation of the SAW, but simply spreads on the wave path. The solution is to reduce the surface energy to move the droplets freely on the surface. Various surface coating technologies have been developed to increase the contact angle of the water droplet. CFx chemical vapour treatment was found to form contact angles larger than 90° and reduce the surface energy significantly [75]. Solution-based Teflon can be applied to the surface of PE substrates to form a hydrophobic surface to provide contact angle larger than 110°. The thickness of the Teflon and CFx layer has to be carefully controlled to reduce attenuation caused by the large acoustic absorption of the layer. Octadecyltrichlorosilane (OTS) was found to form a compact and hydrophobic self-assembled monolayer (SAM) with a thickness less than 10 nm. The OTS layer has a contact angle with water larger than 100° and does not damp the SAW amplitude visibly; therefore it is a good hydrophobic coating for microfluidic applications [70,71].

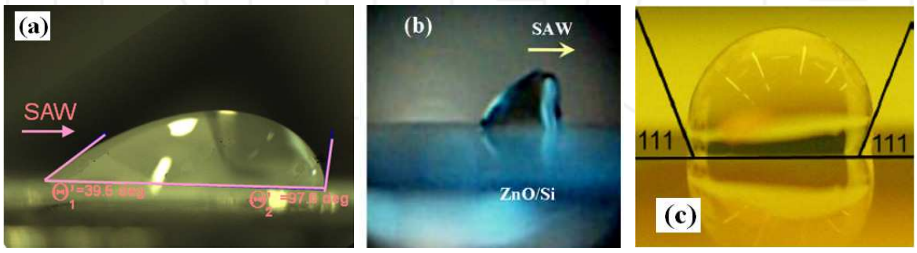

Figure 20. The shape of a droplet under acoustic pressure. The droplet deforms with the leading angle becomes larger and the trailing angle becomes smaller [70]. Reprinted with permission from Institute of Physics, J. Microeng. Micromech. 19, 2009, 035016 for (a) and (c).

Similar to streaming velocity, the droplet moving velocity driven by SAW is found to be proportional to the RF signal amplitude as shown in Fig. 21, and the velocity depends on the droplet size as well as the aperture of the IDT. However, when the droplet diameter is larger than the aperture, further increase in the power does not increase the velocity visibly as the acoustic wave does not fully coupled into the droplets as discussed in [76]. When the aperture is larger than the droplet size, it was found that the velocity decreases with increase of the droplet size as more power is needed to move a larger droplet. As can be seen, the droplet motion velocity is in the range up to 1-2 cm/sec, much larger than the velocities obtained by other methods. Although a SAW can be used to drive droplets at very high speeds, delivery of droplets to required locations with precision is more important for applications in biological analysis than driving the droplets at a high speed. This can be realized by using modulated pulsed RF signal to drive the SAW devices in a controlled manner. By adjusting the period of the on-off RF signal and the signal amplitude, it is possible to move droplets with precision distance. A moving rate of 100 μm/pulse for a droplet of 0.5 μl on a $LiNbO_3$ substrate was obtained by using the pulsed RF signal [77].

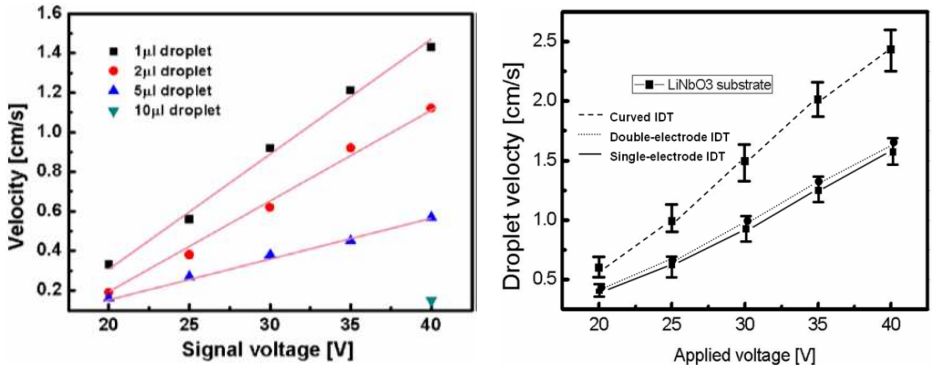

(a) (b)

Figure 21. Droplet moving velocity vs. RF signal amplitude (a) and droplet moving capability vs. IDT structures [70]. Reprinted with permission from Institute of Physics, J. Microeng. Micromech. 19, 2009, 035016 for (a).

As discussed before, the IDT structure significantly affects the energy output, and hence the acoustic streaming and droplet motion owing to its acoustic energy distribution. Generally, a unidirectional IDT has a higher acoustic energy density than a bi-directional IDT, and the curved IDT has the highest energy density. Figure 21b shows a comparison of the droplet motion velocity for SAW devices with different IDT structures. The curved IDT SAW has the highest droplet motion velocity as expected.

3.3. Flexural plate wave micropump and micromixer

Lamb waves have also been utilized for pumping and agitating of minute volumes of liquids [32, 33] and enhancing biochemical reactions [78], based on the fluid motion induced by the travelling flexural wave in a ZnO or AlN piezoelectric membrane [79]. A novel

valveless pump based on a Lamb wave was proposed by Ogawa et al [80]. The liquid in the microchannel was transported by generating a travelling wave on the channel wall, which was composed of a piezoelectric PZT thin film actuator array. A mean flow velocity of about 118 and 172 μm/s was obtained for the 200 and 500 μm wide channels, respectively.

However, due to the low frequency resulting from the thin membrane, the agitation and pumping are too small and insufficient energy is coupled into the liquid. Furthermore, the microfluidic systems contain a membrane vibrating at a high speed, and the yield for fabrication is low, and the reliability of the systems during operation is poor compared to SAW micropumps and mixers. Therefore, research and application of FPW-based microfluidics are currently very limited.

4. Acoustic droplet generator and atomizer

4.1. SAW droplet generator and manipulator

Generation of droplets with volumes from a few *pl*s to a few *μl*s is extremely important for modern biotechnology, life science, medical research and diagnosis. For quantitative analysis in a small volume, it is essential to measure the small volume of reagents and biosamples precisely; otherwise false results can be easily obtained. Although a few technologies have been developed to generate droplets in volumes from a few *nl*s to a few *μl*s, they are difficult to be integrated with microfluidic systems. By changing the acoustic force and hydrophilic and hydrophobic patterns on the surface of a SAW device, it is possible to generate droplets from a few *pl*s to *μl*s on a free surface. Figure 22a is a schematic drawing of a SAW-based droplet generator, consisting of SAW devices with a reservoir and hydrophilic spots surrounded by a hydrophobic surface [49]. When the liquid in the reservoir is pushed forward under the acoustic force, it makes contact with the hydrophilic

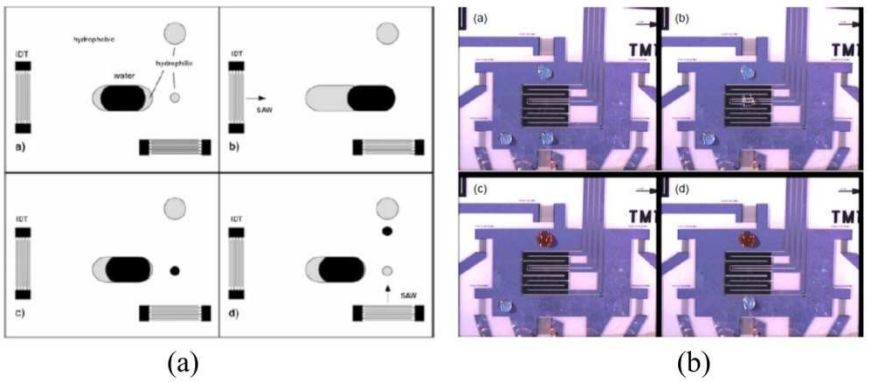

Figure 22. (a) the principle of acoustically driven nano dispenser by selective chemical modification of the wettability of parts of the chip surface and employing two SAW propagating at a right-angle to each other. (b) is a SAW driven microfluidic processor [49]. Reprinted with permission from Elsevier, Superlattice & Microstruct. 33, 2004, 389.

spot and fills it. Once the RF signal is off, the bulk liquid withdraws back to the reservoir as the acoustic force diminishes, leaving the spot filled with the liquid of a fixed volume determined by the size of the spot area and the contact angle. In this way, Woxforth et al. developed a SAW-based droplet generator [49]. Furthermore, by using the virtual containers and tracks formed by hydrophilic surfaces surrounded by hydrophobic surfaces for liquids on a chip, they have developed droplet manipulator and mixer as demonstrated in Fig. 22b.

A combination of a SAW pump with other droplet generators can realize new functions of microfluidics. Electrowetting on dielectrics (EWOD) has been combined with SAW devices to fabricate the EWOD-SAW microfluidics as shown in Fig. 23 [81]. EWOD is used to generate and separate the droplets, while the SAW device is used to move the droplets along the track. The EWOD force is employed to guide and position microdroplets precisely which can then be actuated by SAW devices for particle concentration, acoustic streaming, mixing and ejection, as well as for sensing using a shear-horizontal wave SAW device [82].

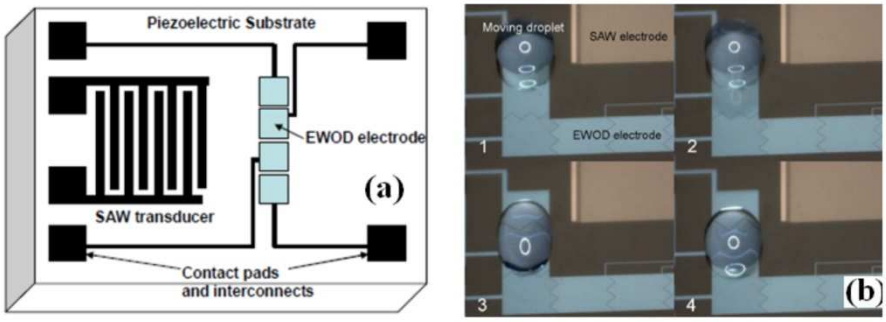

Figure 23. Schematic of integrated EWOD and SAW test structure and the droplet generation by EW and manipulation by SAW [82]. Reprinted with permission from AIP, Biomicrofluidics, 6, 2012, 012812.

4.2. SAW atomizer

If the RF power coupled to the liquid on a hydrophilic surface is sufficiently large, tiny droplets with volumes in the range of a few femtolitres (*fl*s) to *pl*s can be generated and escape from the surface of the host liquid, forming a continuous mist of droplets as shown in Fig. 24. This has been utilized for the development of SAW-based atomizers and droplet generators. Ejection of small particles and liquids has many applications ranging from inkjet printing, fuel and oil injection sprayers and propellers.

The height of the mist is dependent of the RF power applied, and could be up to 6 cm [20,71]. The ejection angle of tiny droplets escaping from the host liquid is determined by the Rayleigh angle, but affected by the RF power and height of the mist [83]. In order to generate a continuous mist on demand, there must be a continuous supply of liquid which can be realized by using a porous structure such as a filter paper linked to a large liquid reservoir as shown in Fig. 25 [65].

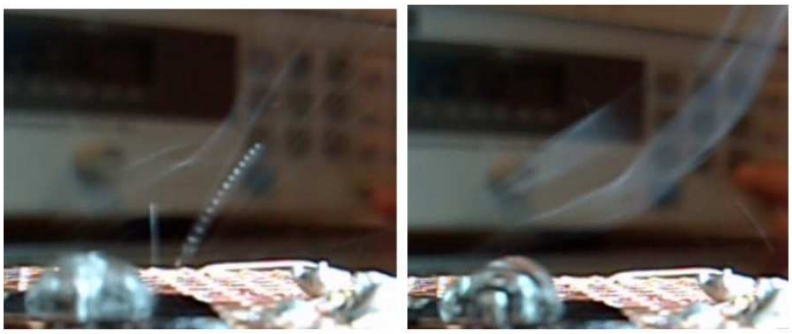

Figure 24. Acoustic streaming induced mist by a ZnO SAW device, which may reach 6mm height.

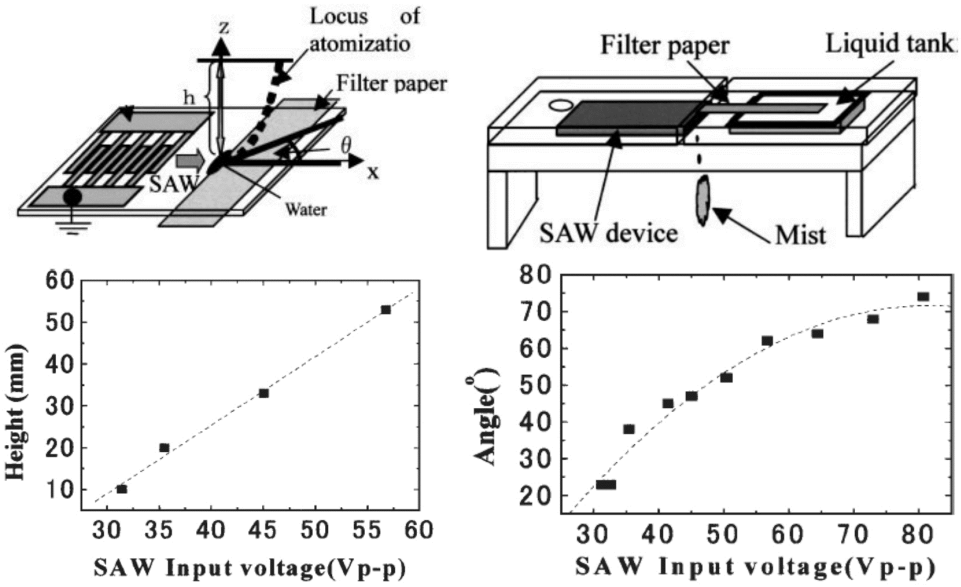

Figure 25. SAW atomization mechanism and setup for the SAW atomizer, and the mist height and angle as a function of SAW input voltage [65]. Reprinted with permission from Japan J. Appl. Phys. Lett. 43, 2004, 2987.

A proper design of SAW ejector can be utilized for nozzle-free ink applications. Tan *et al.* [84] demonstrated another method utilizing two opposite IDTs to converge the acoustic energies at point with a liquid drop ejected perpendicular to the surface, similar to the normal nozzle-based droplet ejector as schematically shown in Fig. 26. The radiation from two sides of the droplet resulted in an elongated liquid column with an angle of about 90°. These SAW ejectors do not have a nozzle head and offer a more cost effective solution when compared to the current ink ejector.

Atomization has been widely applied in pulmonary drug delivery as a promising technology to transport drug formulations directly to the respiratory tract in the form of inhaled particles. The most common methods employed for this application are jet atomization and ultrasonic atomization with difficulties to produce monodispersed particles, i.e. droplets with sizes in the range of 1~5μm in diameter. SAW atomizers are able to produce aerosol droplets with a good particle size distribution. By controlling the RF power applied to the SAW IDT, the droplet sizes can be less than 5 μm [85], suitable for the pulmonary drug delivery application.

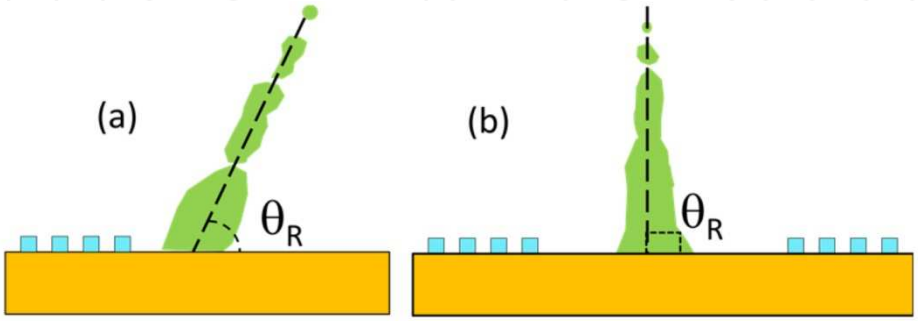

Figure 26. Droplet jetting induced by a single IDT SAW device (a), and droplet jetting induced by a pair of IDT electrodes (b).

Not just bulk SAW devices, but also thin film SAW devices can also achieve a similar atomization effect by using sufficient RF power. Figure 24 shows images of tiny liquid droplets ejected from the surface of a ZnO SAW device obtained by the authors, and the height of the mist is similar to those observed from the $LiNbO_3$ bulk SAW devices, even though thin film SAW devices have lower power delivered compared with the bulk devices.

5. Acoustic wave based biosensors

Most acoustic wave resonators (QCM, SAW and FBAR) can be used as sensors because all of them are sensitive to mechanical, chemical, optical or electrical perturbations on the surface of the devices [86,87]. They are versatile, sensitive and reliable, being able to detect not only mass/density changes, but also viscosity, elastic modulus, conductivity and dielectric properties etc. They have many applications such as sensing pressure, humidity, temperature, strain (stress), acceleration force, vibration, flow, pH values, radiation, electric fields etc. They are sensitive gas sensors once combined with specific gas absorption layers [88,89,90]. Development of acoustic wave based biosensors is relatively new but has a huge potential as they can detect tiny traces of biomolecules [22,23]. This can be utilized to detect viruses and genetic disorders, diagnose early stage diseases and cancers [91,92]. The principle of acoustic biosensors is similar to those of other biosensors, which are based on a specific interaction between biomarkers (also called probe molecules) deposited on the surface of the sensors with target molecules in the biosamples. Compared with other

common biosensing technologies, such as surface plasmon resonance (SPR), optical fibres, and field effect transistors or cantilever-based sensors, acoustic wave based sensors have the combined advantages of simple operation, high sensitivity, small size, compact and low cost. In the following section, highlight the acoustic wave sensor technologies.

5.1. QCM sensors

Although the piezoelectric effect was discovered in the late 19th Century, quartz crystal resonators only found widespread applications in electronics, material and biological researches when it was demonstrated that there was a linear relationship between mass adsorbed on the surface and the resonant frequency of the crystal in 1959 by Sauerbrey [93]. Biosensing became possible when suitable oscillator circuits for operation in liquids were developed [94]. The QCM is one of the most developed biosensors that can be operated in a liquid environment using the thickness shear-mode. A QCM consists of a bulk piezoelectric material with typical dimensions of 1 cm in diameter and 500-1000 μm in thickness, sandwiched between two metal electrodes. When an A.C. electrical signal is applied to the two electrodes, it excites a standing wave between the two electrodes through the PE effect. The operating frequency of the QCM is determined by the thickness of the PE-layers, and is typically 5, 10 and 20MHz. As shown by eq.(1), the sensitivity of acoustic resonators is determined by the square of the frequency and the base mass. With decreasing thickness of the Quartz layer, the frequency of the QCM has been increased significantly, thus its sensitivity has been dramatically increased. There has been intensive research recently to develop thin film based QCMs with operating frequencies of several hundreds of MHz [37,38] which demonstrated their great potential for biosensing with better sensitivity.

For biosensing, QCM biosensors have been used to detect the interaction between protein-protein, DNAs, protein-DNA, viruses, bacteria etc, and demonstrated their usefulness, versatility and robustness with high sensitivity. For practical applications, more QCM sensors have been integrated with other structures and devices such as molecular imprint polymers [95], sensors [96] and microfluidics [97] for multi-task detection and monitoring with better accuracy and more functionality. There are hundreds of published papers on QCM biosensors; a review of QCM biosensors is beyond the scope of this book chapter. Readers can find more information in refs. [98,99].

5.2. SAW sensors

SAW devices are not only used for microfluidics, but are very good sensors. Since SAW devices have a much smaller active mass and much higher operating frequency than those of QCMs, the sensitivity of the SAW devices increases dramatically as shown in Fig. 3. Furthermore by using advanced photolithograph technology, especially e-beam writing techniques, it is now possible to fabricate SAW devices with operating frequencies up to the Gigahertz [100,101], and the sensitivity of SAW sensors can be further increased.

The longitudinal mode SAW device has a substantial surface-normal displacement that rapidly dissipates the acoustic wave energy into a liquid, leading to excessive damping, and

hence poor sensitivity and noise for biodetection in liquid. Shear horizontal (SH-) mode SAW devices have substantially reduced coupling of acoustic energy into the liquid [102,103], hence they can maintain a high sensitivity in liquids. Consequently SH-SAW devices are suitable for biodetection, especially for "real-time" monitoring of physiological conditions of a patient. To further reduce the base mass of a SAW device to improve the sensitivity, Love wave SAW devices have been developed which consist of a normal SAW device and a thin wave guide layer (typically sub-micrometers) such as SiO_2 and polymers on top of the SAW surface. Since the acoustic velocity is slow in the wave guide layers, acoustic waves are trapped in the thin wave guide layer, resulting in a drastically reduced base mass and significantly improved sensitivity and quality of the sensors [104,105]. They are therefore frequently employed to perform biosensing in liquid conditions [106,103].

For LOC applications, integratable thin film SAW sensors are more attractive and desirable. A lot of efforts have been made to develop AlN and ZnO thin film SAW sensors. A ZnO/Si SAW device has been successfully used in the detection of aminohexanoic acid succinimidyl ester (DNP-X) and anti-DNP-KLH antibody [107]. The resonant frequency of the ZnO SAW devices was found to shift to lower frequencies as the PSAs are specifically immobilized on the surface-modified ZnO SAW device. A linear dependence has been measured between the resonance frequency change and the anti-DNP concentration over a range from 2 to 1000 ng/ml, and saturated as the concentration increases further due to the reduction of binding sites [107].

To realize biosensing in liquids with better sensitivity, Love wave SAWs have been studied intensively. ZnO has a shear wave velocity of ~2600 m/s, whereas that of ST-cut-quartz is about 4996 m/s. Therefore, it is reasonable to use ZnO as a guiding layer on substrates of ST-cut quartz to form Love mode biosensors. The other potential substrate materials for Love-mode ZnO sensors include $LiTaO_3$, $LiNbO_3$ and sapphire. A ZnO Love mode device of ZnO/ST-cut quartz has a maximum sensitivity up to ~18.77×10^{-8} m^2 s kg^{-1}, much higher than that of a SiO_2/quartz Love mode SAW device [108,109]. Mchale et al recently reported ZnO/SiO_2/Si SAW Love mode sensors with a sensitivity of 8.64 μm^2/mg [110], which is about 2 to 5 times that of ZnO/$LiTaO_3$ [111] and SiO_2/quartz Love sensors [112]. Another promising approach for making a ZnO based Love mode sensor is to use a polymer film (such as PMMA, polyimide, SU-8 or parylene C) on top of the ZnO layer as the guiding layer. However, this layered structure uses a polymer waveguide and has a relatively large attenuation compared with those of solid waveguide layers.

AlN SAW devices have higher acoustic velocities, for example, about 6000 m/s shear velocity for an AlN/Si SAW device, and thus it is desirable to use AlN SAW devices for sensors for high sensitivity. However there are not many reports on AlN based SAW biosensors. The reason could be the difficulties in the deposition of the thick AlN film (>4 μm) required for high quality SAW device fabrication. They normally have a large film stress and poor adhesion with the substrate. Although AlN films deposited to deposit on a $LiNbO_3$ substrate have been reported to form a highly sensitive Love mode sensing devices [113,114].

5.3. FBAR sensors

FBARs were initially developed as high frequency resonators for applications in electronics as filters, duplexer etc in 1980s' [25,26]. FBARs have been considered for biosensor application since 2000, and are considered as one of the most advanced sensors with extremely high sensitivity and very small dimensions. As the wavelength of the bulk resonators is determined by the thickness of the PE-layer, it is normal to fabricate FBARs with thin PE-layers. FBARs typically have frequencies of a few GHz, and ones with f_r of 8 GHz or higher have been demonstrated [115,116]. Owing to the small base mass and high operation frequency, attachment of a small amount of target mass is able to induce a large frequency shift – typically a few MHz. This improves the sensitivity and makes the signal easily to be detected using simple electronic circuitry. Although the sensitivity of FBARs is not as good as predicted by eq.(1), it is still about three and two orders of magnitude higher than those of QCMs and SAWs respectively as shown in Fig.4 [28,117].

A ZnO-based label free FBAR biosensor with an operating frequency of 2 GHz was used to detect DNA and protein molecules [115]. It showed a sensitivity of 2400 Hz·cm^2/ng, which is approximately 2500 times higher than a conventional QCM device could achieve. A recent Al/ZnO/Pt/Ti FBAR design also showed a sensitivity of 3654 Hz·cm^2/ng with a better thermal stability than that of ZnO-based FBARs [118,119].

Based on eq.(1), an increase in f_r would make FBARs of higher sensitivity. However it should be pointed out that the limitation to the sensitivity of acoustic resonators, especially the FBARs, is not only the frequency, but also the quality factor. It is easy to make FBARs of high f_r by using a thin PE layer, but the quality factor of the FBARs was found to decrease dramatically with decrease of the thickness of the PE-layer, mostly due to the relatively poor crystal quality, small grain size, poor thickness uniformity, rough surfaces and the existence of a thick transition layer (20-80 nm), resulting in a severely reduced quality factor when a thin PE layer is used. Also it was found that the electrode shape and material properties also significantly affect the quality factor. Electrodes with 90° regular angles reflect the surface travelling wave and deteriorate the Q-factor. Electrodes with high acoustic impedance and low mass are preferred for fabrication of high performance FBARs. Aluminium is one of the most popular electrode materials in the microelectronics industry. It has a low mass density, but the acoustic impedance is low and thus is not the best material for the fabrication of FBARs. Au, Pt and W have high acoustic impedance but their mass densities are high, leading to large mass loading effects. A carbon nanotube (CNT) layer was found to be the best electrode material for FBARs as it has a high elastic modulus and low density (hence a high acoustic impedance and low mass loading) and CNTs have thus been used for fabrication of FBARs with much improved quality factor. An improvement of Q-value by 5 times was demonstrated simply by using a CNT layer on top of existing metal electrodes [120]. Garcia-Gancedo et al recently fabricated FBARs with CNT layer as the top electrode and demonstrated FBARs with a quality factor over 2000 [121,122], one of the best values reported. Also the spurious ripples round a resonant peak found in Au electrode FBARs disappeared when CNTs were used as shown in Fig. 27. The FBARs with CNT electrodes

showed a better sensitivity than the Au electrode ones with a mass detection limit down to 10^{-13}g, with the potential to go down to 10^{-15}g, suitable for detecting a single molecule.

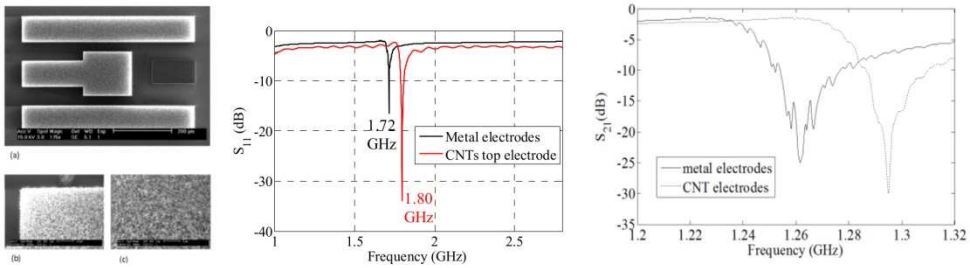

Figure 27. (a) SEM images of a fabricated SMR with CNTs layer top electrode. The middle is a typical frequency response, showing the main resonance at 1.75 GHz. The ripples for FBARs made of Au and CNTs top electrode. It disappears in CNTs-FBARs due to high acoustic impedance [122]. Reprinted with permission from Elsevier, Sensors and Actuators, B 160, 2011, 1386.

The majority of the PE thin films have crystal orientation (0002) normal to the surface of the substrates. They are suitable for fabrication of FBARs with longitudinal mode and appropriate for gas phase detection. FBARs with protein functionalized surfaces have been used as a gas phase biosensors, and demonstrated their feasibility for sensing an odorant binding protein of AaegOBP22 using N,N-diethyl-meta-toluamide (DEET) as the ligand to the odorant binding protein [123]. For sensing in liquids, novel structures, especially integrated with microfluidics, is needed. Zhang et al performed biodetection in liquids by taking advantage of the back trench structure. The trench was used as a container in which the bioreaction could take place, while a FBAR on the other side of the thin membrane was used for sensing. This demonstrated its feasibility for biodetection [124]. Similarly Wingqvist et al. used the surface of a FBAR for sensing with a built-in microchannel on the back which allows continuous flow of the biosamples or buffer solution to pass for a continuous measurement [31]. A schematic drawing is shown in Fig. 28.

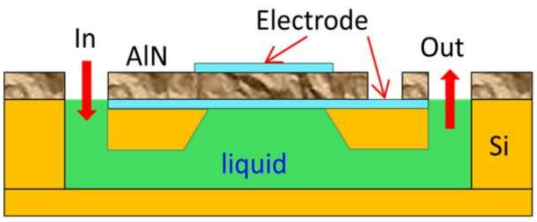

Figure 28. Typical structure of lateral field excited inclined AlN film FBAR.

For direct liquid contact sensing, it is necessary to develop ZnO or AlN films with crystal orientation inclined relative to the surface normal, allowing generation of shear waves to be used for detection in a liquid [125]. A (1120) textured ZnO film exhibits pure shear mode waves which can propagate in a liquid with little damping effect. A ZnO shear mode FBAR

device has been used in a water-glycerol solution, with a high f_r of 830 MHz and a sensitivity of 1000 Hz·cm²/ng [126]. Weber et al. fabricated ZnO FBAR devices using a ZnO film with 16° off c-axis crystal orientation, which operated in a transversal shear mode [125]. For an avidin/anti-avidin system, the fabricated devices had a high sensitivity of 585 Hz·cm²/ng and a mass detection limit of 2.3 ng/cm². The shear wave FBAR devices also showed a more stable temperature coefficient of frequency [30,31].

Another method for liquid phase biodetection is to use the lateral field excitation (LFE) for FBARs as shown in Fig. 29. This structural FBAR requires both signal and ground electrodes being in-plane and parallel on the exposed surface of the PE films [127,128,129]. Since the excitation is parallel to the surface and perpendicular to the normal c-axis crystal orientation, the FBARs exhibit a thickness shear mode operation. The devices are stable in biologically equivalent environments [130,128]. However, lateral structural FBARs normally have a low quality factor and the mechanism of the exciting resonance is not fully understood yet. A lot of research is needed before they can be effectively used as sensors. Furthermore, lateral FBARs have a very narrow active area, and it is difficult to incorporate microfluidics within the narrow channel for sensing.

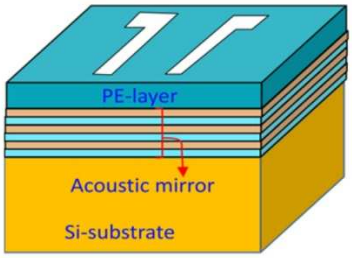

Figure 29. Schematical structure for the lateral field excited FBAR devices, which generates a thickness shear mode resonance.

5.4. Flexural plate resonant sensors

Lamb wave devices on a membrane structure have been used for biosensing in liquid [34]. Since the propagation velocity of the Lamb wave in the membrane is slower than that in the fluids on the surface, the acoustic energy is not easily dissipated, thus the Lamb wave sensors can be used for thus applications [131]. Since the resonant frequency of the FPW devices is small, it is not sensible to use the frequency as the parameter for sensing due to poor sensitivity as indicated by eq.(1), the amplitude of the resonant wave is normally used for sensing in liquid. Therefore, the sensitivity of these devices increases as the membrane thickness becomes thinner [35, 15].

A ZnO based FPW device has been used to monitor the growth of bacterium "Pseudomonas putida" in a boulus of toluene and the reaction of antibodies in an immunoassay for an antigen present in breast cancer patients [132]. $Si/SiO_2/Si_3N_4/Cr/Au/ZnO$ FPW devices have

been used for detecting human IgE based on the conventional cystamine SAM layer technology with a sentivity of 8.52×10^7 cm^2/g at a wave frequency of 9 MHz [133]. However, the FPW biosensor has not been widely reported because of the low sensitivity, difficulty of fabrication and high temperature sensitivity of the thin film.

6. Other SAW-based functions and lab-on-a-chip

Since the acoustic wave mechanism can be utilized for fabrication of various microfluidic devices and sensors, it would be very attractive to fabricate single acoustic wave mechanism-based lab-on-chip systems [117]. Development of such systems has been rather limited so far, as the individual acoustic technologies are yet to be fully explored, developed and optimized. Current activities have been focused mainly on the development of individual acoustic wave based devices and systems such as acoustic microheater, SAW-based polymerase chain reaction (PCR), SAW-based particle concentrator, sorting and delivery devices etc. These will be highlighted in this section.

6.1. SAW microheater

For SAW devices, an input of high RF power will induce acoustic heating through crystal vibration and absorption of acoustic energy by defects in the substrates. For sensing, the input RF signal normally has a low power and acoustic heating is not a problem. For acoustic microfluidics, especially droplet-based pumps, acoustic heat may increase the surface temperature of the SAW device over 100 °C which will damage most of the cells and bio-molecules and reduce their biological integrity. Acoustic heating can be suppressed by using a pulsed RF signal to maintain the temperature below 40 °C. Although acoustic heating has many negative effects for biological and electronic applications, controlled acoustic heating can be utilized as a remote microheater for many applications, such as in polymerase chain reaction (PCR) to amplify DNA concentration for detection or to accelerate bioreaction.

Figure 30 shows the surface temperature as a function of RF signal voltage measured for a ZnO thin film SAW device. The temperature at a position 5 mm away from the IDT on the wave path was monitored. The temperature increases with the signal amplitude and the duration of the RF signal, and decreases with the distance from the IDT [77]. The maximum temperature can reach at 140 ^oC for a signal voltage of 60 V. The temperature was found to have a distribution along the wave path. It is higher near the IDT, and decreases away from the IDT due to attenuation of the wave. Acoustic heating has been utilized to construct PCR as will be discussed later [74,134]. For normal gas sensing, initialization of sensors requires a high temperature to remove all absorbed substances. Acoustic heating could be utilized for self-initialization for SAW gas sensors without need of an additional microheater, which greatly simplifies the system and reduces the cost and fabrication process. Effective utilization of acoustic heating would generate compact, useful microsystems with many functions, and many applications are yet to be explored.

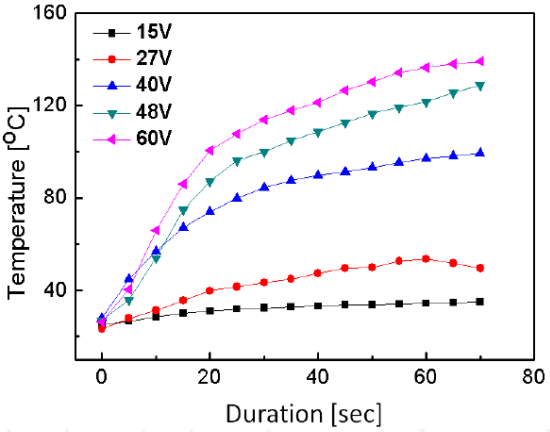

Figure 30. Acoustic heating induced temperature rise as a function of RF signal duration by a SAW microheater [77]. Reprinted with permission from AIP, J. Appl. Phys, 105, 2009, 024508.

6.2. SAW particle concentrator

Transportation and concentration of particles or bio-substances such as cells are important issues for biological applications. As above, the SAW acting on the edge of a droplet can generate a shear force within the droplet. This shear force can generate circulating streaming, moving particles towards the centre as shown in Fig. 31. From a side view, the fluid can be observed to be pushed upward just above the SAW propagation area which results in primary azimuthal rotation within the droplet periphery. Raghavan et al [135] reported that the flow phenomenon within liquid droplets due to SAW asymmetric positioning are similar to that obtained by the flow field between stationary and rotating disks. This azimuthal rotation phenomenon has been utilized for particle concentration.

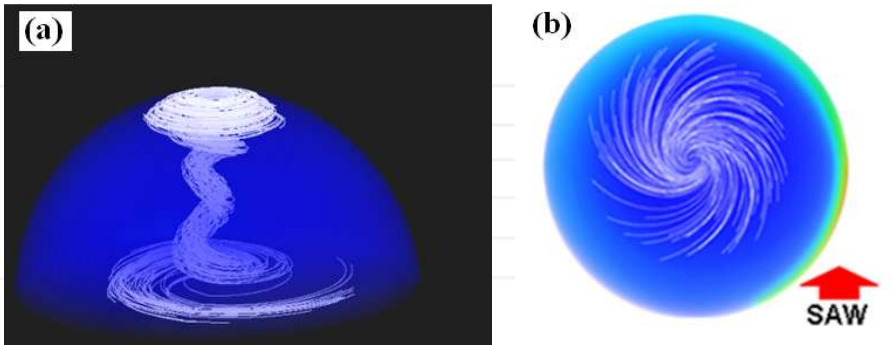

Figure 31. Side view (a) and overview (b) of simulated circulating streaming patterns induced by acoustic wave for a 10μl droplet [53].

Figure 32 shows the frame images of starch particles captured during the concentration process within a 20 μl droplet after applying an RF signal to the IDT electrode for a few

seconds. Initially, the particles are uniformly dispersed in the water, and circulating streaming is induced once the RF signal is applied. The flow circulation rapidly establishes a particle cluster towards the centre of vortex, in the form of a conical shape similar to that depicted theoretically. The shear force induced particle migration is due to the gradient in the azimuthal streaming velocity in the droplet, resulting in particle motion from a higher shear force area at the droplet periphery to a lower shear force area at the bottom of the droplet centre. The shear velocity is large on the edge of the droplet, and gradually decreases on approaching the centre of the droplet. The particles circulate with the liquid in the droplet and simultaneously migrate from the high to the low shear velocity regions [53,136]. The concentration effect is dependent of the RF power as well as the properties of the particles. At a low power, it is not sufficient to generate a gradient in the azimuthal streaming velocity, whereas a high power produces a strong turbulent streaming, dispersing particles within the droplet randomly without any concentration effect [53]. The particle size is also critical for the efficient concentration. Particles with certain sizes can be easily agglomerated, whereas small particles can flow inside the liquid for very long time before being forced into the central region. Therefore it is possible to utilize this to separate particles with different sizes using a SAW device.

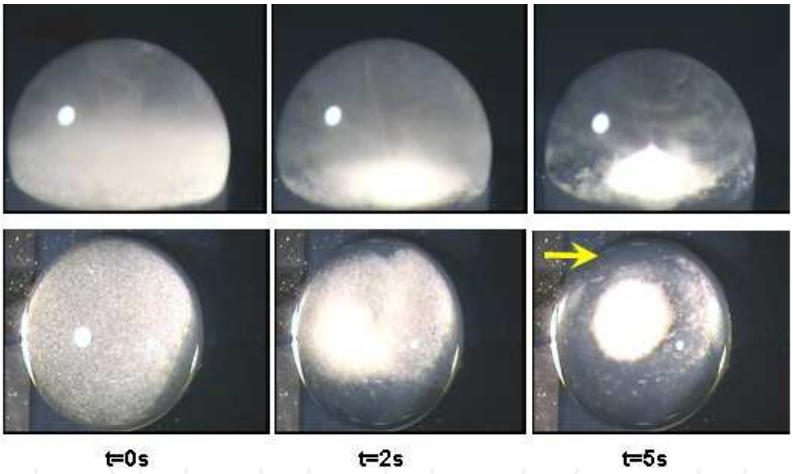

Figure 32. Captured video images illustrating the rapid starch particles concentration process for a 30 μl droplet. The first row shows a side view, while the second row a top view. The yellow arrow is the SAW propagation direction [53]. Reprinted with permission from Institute of Physics, J. Microeng. Micromech. 21, 2011, 01500581.

6.3. Particle sorting and manipulator

Particle sorting, separation and counting are frequently used in biological and medical analysis. Biological samples contain various cells such as blood plasma, and red and white cells. For analysis, these cells are to be separated and counted. Cell separation and counting are powerful tools being used for quantitative analysis. Acoustic waves can be utilized for

particle sorting, separation, counting etc, mostly relying on the nodes and antinodes generated by standing waves [137]. Figure 33 shows the principle of a SAW-based particle sorting device. A pair of IDTs is arranged face to face with a distance between them equal to an integer of the half wavelength, nλ/2. Upon application of an RF signal, standing waves between the two IDT electrodes can be formed. If a channel is fabricated perpendicular to the wave path of one wavelength wide, the pressure node in the channel will confine the particles within the pressure node, generating streaming with particles confined within the line.

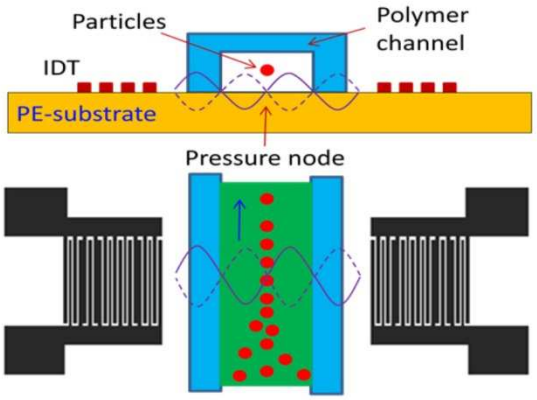

Figure 33. Formation of pressure node and anti-node by standing waves used for focusing particles inside a channel. A single wave node in a PDMS/SAW device and focus of the particles in a line.

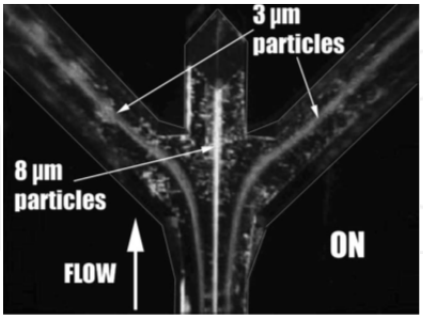

Figure 34. Microscope image of microparticle line induced by acoustic wave node [137]. Reprinted with permission from RSC Publishing, Chem. Soc. Rev. 36, 2007, 492.

Shi *et al*. employed this scheme to obtain focused particle lines using PDMS as the microchannel wall [138]. They have demonstrated fluorescent polystyrene particles sorting for a solution with a density of 1.176×10^7 beads/*ml*. The particle size is around 1.9 μm, and the flow containing the particles passes through a channel, and eventually forms a stable particle flow. By incorporating channels with different exits, particles with different sizes can be separated. Fig. 34 is the photo image of the particles captured by a camera [138].

It should be pointed out that standing waves have a long range force compared with the sizes of the microparticles; therefore it should be considered as a coarse manipulator or tweezers, suitable for simultaneous handling of a large group of particles or cells. It would be difficult to manipulate particles precisely down to the micrometre scale individually. For precision manipulation of particles, it would be best to integrate acoustic wave devices with other mechanisms. Wiklund et al [139] has integrated dielectrophoretic microfluidics mechanisms with ultrasonic particles concentrators. The ultrasonic standing wave delivers a long range force for high through-put particle manipulation, while the short-range dielectrophoretic forces are used for precision control to realize individual cell manipulation for bioanalysis.

Acoustic forces can be utilized to drive particles to places in order to realize scaffolding for cell growth. An in vitro cell culture is a technique used to grow cells in extra-cellular matrices and potentially for organ farming. Successful growth of cells depends on uniform distribution of seed cells into the scaffold of the matrices and the efficiency of the seeding process. The moving of a cell suspension into the scaffold material, typically a polymer, in the absence of external driving forces is exceptionally slow due to the large capillary resistance which may take from hours to days. SAW device can move a droplet with strong internal streaming and agitation as discussed, and can be used to deliver particles into the polymer matrices for cell growth. Yeo at al. have investigated the effect of SAW agitation on the efficiency of suspended fluorescence particles in a polycaprolactone (PCL) scaffold [140]. They demonstrated that efficiency up to 90% can be achieved on a SAW device within a few seconds, and the particles are uniformly distributed within the polymer matrix [140].

6.4. Other acoustic wave based functions

The acoustic wave technique has been used for biodegradable polymeric nanoparticle generation [141]. A polymeric incipient was dissolved into a solvent drop, and then atomized by a SAW. The solidified polymeric particles left behind are monodispersed. With this technique, 150–200 nm polymer spherical clusters were formed with sub-50 nm particulates. Periodically ordered polymer has also been patterned on a substrate by SAW atomization [142]. When a polymer solution was spread over the surface of a SAW device with two IDTs perpendicular to each other, the surface displacements induced by the standing waves displace the polymer film, breaking up the film in both the transverse and longitudinal directions producing evenly spaced solidified polymer microstructures. The spaces between the nanostructures in the X and Y-directions are approximately half the SAW wavelength in both directions with a pattern as shown in Fig. 35(left) schematically.

This can also be utilized to fabricate fine microwires of soft matter with nanoparticles uniformly dispersed in a solvent.

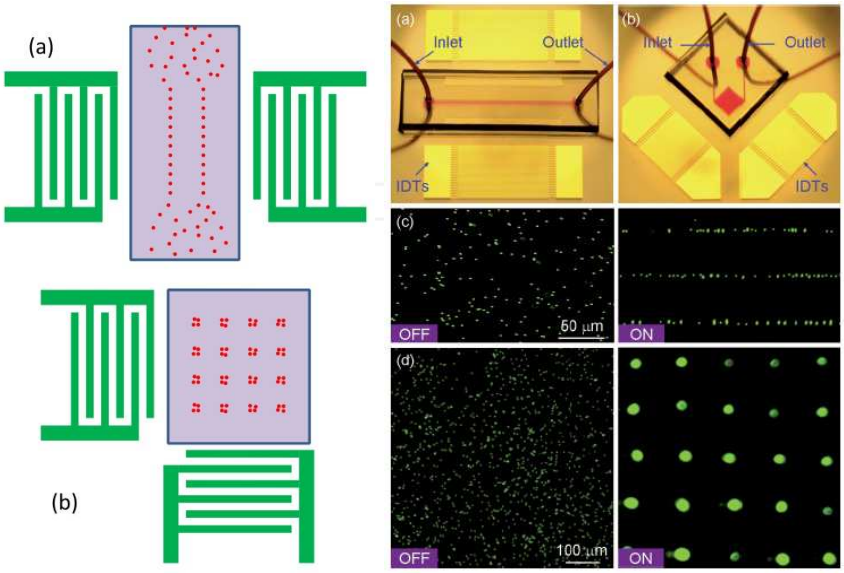

Figure 35. (Left) Particle lines formed in a fluid induced by standing waves from a pair of SAW IDTs; (Right) 2D array of particles form by a pair of IDTs in perpendicular [138]. Reprinted of (b) with permission from RSC Publishing, Lab on Chip, 9, 2009, 2890.

6.5. SAW based lab-on-a-chip

By using a combination of streaming induced mixing, enhanced biochemical reaction, droplet delivery and cell sorting etc by acoustic waves with other microfluidic and sensing functions, people have realized SAW based LOCs for various applications. A PCR system based on the combination of a SAW and resistance microheaters has been developed [74,134]. A schematic of the suggestion is shown in Fig. 36. The SAW-PCR system is a droplet-based DNA amplifier with droplets of the sample embedded in oil. SAW devices are used for moving and aligning the droplets between the zones with different temperatures through virtual tracks formed by chemical modification of the surface hydrophobicity. Once PCR amplification is completed, the droplet is moved to another heater for hybridization.

The chip is able to perform a fast and specific PCR with a small volume of 200 *nl* within 10 min. A single nucleotide polymorphism (SNP) responsible for the Leiden Factor V syndrome from human blood was successfully amplified by the PCR system and detected [134]. A SAW-based chip has several advantages over microfluidic channel systems. It can avoid the problems of clogging, large pressure drop and vaporization of liquid from the solid surface. Furthermore, the SAW streaming can also help to speed up the binding reaction and to get a more homogeneous fluorescence in hybridization.

Furthermore, attempts have been made to develop stand alone biodetection systems with integrated SAW microfluidics and sensors. In these cases, SAW microfluidics is mainly used for transporting liquid and agitating to minimize non-specific binding and speed-up the reaction. Due to the small dimensions, liquid in microchannels is dominated by a laminar flow, and the biochemical reaction is limited to mass transportation. The process is very slow, and the reaction is incomplete, thus additional agitation to speed up the reaction is therefore required. A SAW device is an ideal planar device to be integrated in the system for these purposes. Figure 37 is a schematic drawing of a SPR detection system with integrated SAW microfluidics [143]. By utilizing the abilities of moving droplets and acoustic streaming by SAW device, a droplet based SPR system for real-time sensing was realized.

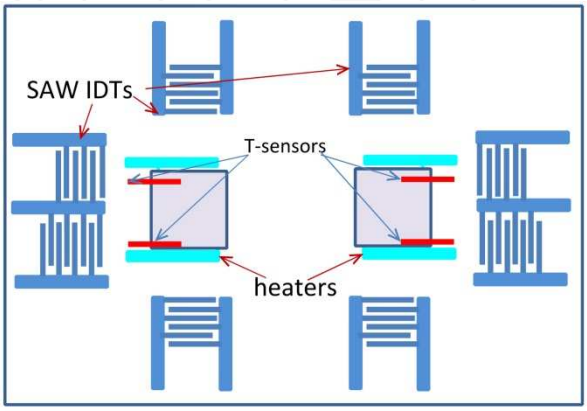

Figure 36. A schematic drawing the SAW based PRC system.

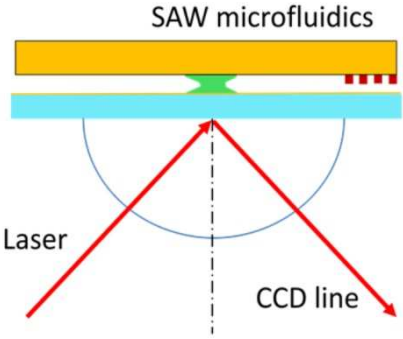

Figure 37. Schematic drawing of the set-up of the droplet-based SPR with SAW integrated for streaming to allow the real time monitoring of interactions.

7. Conclusions

Lab-on-a-chip systems for medical research, drug development and healthcare etc typically consist of a set of microfluidics and sensors. In most cases, the mechanisms for microfluidics

and sensors are different and these devices are mostly assembled together to form LOCs, making the LOCs big and difficult to operate. Acoustic wave based lab-on-a-chip systems are a miniaturized microsystems with typical sizes of few square centimetres. LOCs may provide a single or multi-function such as transporting biosamples and sensing on a single chip.

Bulk and surface acoustic waves have found tremendous applications in LOCs. Surface acoustic waves have strong forces and can be utilized for fabrication of micropumps, mixers, droplets and mist generators for handling liquids and biosamples effectively and efficiently. On the other hand, bulk and surface acoustic wave based resonators (QCMs, SAWs and FBARs) are extremely sensitive to traces of absorbed mass and hence can be utilized for development of high sensitivity biosensors. Also acoustic waves can be utilized for generating many other functions such as remote heating, cell concentration and delivery. These unique functions of acoustic waves make it possible to develop lab-on-a-chip systems with a single actuation and sensing mechanism. Furthermore all these acoustic devices can be realized by using thin film technology, hence opening the way for integration of acoustic wave based LOCs with Si-based electronics on the same substrate.

Author details

J. K. Luo
Dept. Info. Sci. & Electron. Eng., Zhejiang University, China
Inst. Of Renew. Energy & Environ. Technol., Bolton University, UK

Y. Q. Fu
Thin Film Centre, University of West of Scotlant, Paisley, Scotland

W. I. Milne
Dept. of Eng. University of Cambridge, UK

Acknowledgement

The authors would like to acknowledge the partial financial support from the Leverhulme Trust under the grant No. of F/01431, The Knowledge Centre for Materials Chemistry under Grant No. of X00680PR, Canergie Trust Funding and Royal Society of Edinburgh, the Natural Science Foundation of China (No. 61274037) and Zhejiang Provincial Natural Science Foundation, China (No. Z1110168).

8. References

[1] Nguyen N T, Huang X and Chuan T K; J. Fluids Eng. 124; 2002; 384.
[2] Laser D J and Santiago J G; J. Micromech. Microeng. 14; 2004; R35.
[3] Woias P; Sens. Actuat. B105, 2005, 28.
[4] Truong T Q and Nguyen N T; J. Micromech.Microeng. 14, 2003, 632.
[5] Cho S K, Moon H and Kim C-J; J. Microelectromech. Syst. 12, 2003, 70.

[6] Lacharme F. and Gijs M A; SensorsActuators A 117, 2006, 384.
[7] Darabi J, Rada M, Ohadi M and Lawler J; J. Microelectomech. Syst. 11, 2002, 684.
[8] Jones T B; J. Electrostat. 51/52, 2001, 290.
[9] Pollack M G, Fair R B and Shenderov A D; Appl. Phys. Lett. 77, 2000, 1725.
[10] Pollack M G, Shenderov A D and Fair R B; Lab Chip 2, 2002, 96.
[11] Torkkeli A, Saarilahti J, Haara A, Harma H, Soukka T and Tolonen P; Proc. IEEE MEMS. pp.475–78, 2001.
[12] Mugele F and Herminghaus S; App. Phys. Lett. 81, 2002, 2303.
[13] Luo J K, Fu Y Q, Li Y, Du X-Y, Flewitt A J, Walton A J and Milne W I, J. Micromech. Microeng. 19, 2009, 054001.
[14] Chao C, Cheng C H, Liu Z B, Yang M, Leung W F; Proc. IEEE Int. Ultrason. Symp. 2008, pp.521.
[15] Luginbuhl P, Collins S D, Racine G A, Gretillat M A, De Rooij N F, Brooks K G and Setter N; J. Microelectromech. Syst. 6, 1997, 337.
[16] Kwon J W, Yu H, Zou Q, Kim E S; J. Micromech. Microeng. 16, 2006, 2697.
[17] Wixforth A, Strobl C, Gauer C, Toegl A, Scriba J and Guttenberg Z V; Anal. Bioanal. Chem. 379, 2004, 982.
[18] Friend J R and Yeo L Y, Rev. Modern Phys. 83, 2011, 647.
[19] Yeo L Y and Friend J R, Biomicrofludics, 33, 2009, 012002.
[20] Fu Y Q, Luo J K, Du X Y, Flewitt A J, Li Y, Markx G H, Walton A J and Milne W I, Sens. Actuat. B143, 2010, 606.
[21] Lange K, Rapp B E and Rapp M; Anal. Bioanal. Chem. 391, 2008, 1509.
[22] Shiokawa S, Kondoh J; Jap. J. Appl. Phys., 43, 2004, 2799.
[23] Ballantine D S Jr, White R M, Martin S J, Ricco A J, Frye G C, Zellars E T, Wohltjen H; 1997. Acoustic Wave Sensor—Theory, Design, and Physico-Chemical Applications, Academic Press, San Diego.
[24] Buttry D A and Ward M D; Chem. Rev. 92, 1992, 1355.
[25] Lakin K M and Wang J S; Appl. Phys. Lett. 38, 1981, 125.
[26] Lakin K M; IEEE Trans. Ultrason. Ferroelectr. & Freq. Control, 52, 2005, 707.
[27] Ruby R; Proc. IEEE Ultrasonics Symp., 1-6, pp.1029-1040, 2007
[28] Rey-Mermet S, Bjurstrom J, Rosen D and Petrov I; IEEE Trans. Ultrason. Ferroelectric and Freq. Control; 51, 2004, 1347.
[29] Kang Y R, Kang S R, Paek K K, Kim Y K, Kim S W and Ju B K, Sens. & Actuat. A117, 2005, 62.
[30] Link M, Schreiter M, Weber J, Gabl R, Pitzer D, Primig R, Wersing W, Assouar M B and Elmazria O; J. Vac. Sci. Technol. A24, 2006, 218.
[31] Wingqvist G, Bjurstrom J, Liljeholm L, Yantchev V and Katardjiev I; Sens. & Actuat. B123, 2007, 466.
[32] Nguyen N T and White R MSens. & Actuat. 77, 1999, 229.
[33] Meng A H, Nguyen N T and White R M, Biomed. Microdevice, 2:3, 2000, 169.
[34] Muralt P, Ledermann N, Baborowski J; IEEE Trans. Ultrason. Ferroelectr. Freq. Control. 52, 2005, 2276.

[35] Nguyen N T and White R M; IEEE Trans. Ultrason. Ferroelect. Freq. Control. 47, 2000, 1463.
[36] Lucklum R and Hauptmann P; Meas. Sci. Technol. 14, 2003, 1854.
[37] Kao P, Doerner S, Schneider T, Allara D, Hauptmann P and Tadigadapa S, J. Microelectromech. Syst. 18, 2009, 522.
[38] Kao P and Tadigadapa S, Sens. & Actuat. A149, 2009, 189.
[39] Wu T T and Wang W S; J. Appl. Phys. 96, 2004, 5249
[40] Benetti M, Cannatà D, Pietrantonio F D and Verona E, Proc. IEEE Ultrason. Symp. pp.1738, 2003.
[41] Hachigo A, Nakahata H, Itakura K, Fujii S and Shikata S, Proc. IEEE Ultrason. Symp. pp.325, 1999.
[42] Wixforth A; J. Associat. Lab. Automat., 11, 2006, 399.
[43] Josse F, Bender F and Cernosek R W; Anal. Chem. 73, 2001, 5937.
[44] Rayleigh L; On the circulation of air observed in Kundt's tubes, and on some allied acoustical problems, Trans. R. Soc. 25, 1884, 224.
[45] Westervelt P J; J. Acoust. Soc. Am. 25, 1953, 60.
[46] Nyborg W L; Acoustic streaming Physical Acoustics, Edited by W P Mason (New York: Academic) 1965, pp.265–331
[47] Shiokawa S, Matsui Y and Ueda T; Proc. Ultrasonic Symp. pp. 645, 1989.
[48] Nyborg W L Acoustic streaming Nonlinear Acoustics, Edited by M F Hamilton and D T Blackstock (New York: Academic), pp.207–331, 1998
[49] Wixforth A; Superlattices & Microstruct. 33, 2004, 389.
[50] Shiokawa S, Matsui Y and Morizum T, Jpn. J. Appl. Phys. 28, 1989, 126.
[51] Shiokawa S, Kondoh J; 2004. Jap. J. Appl. Phys. 43 2004, 2799.
[52] Frommelt T, Gogel D, Kostur M, Talkner P, Hanggi P; IEEE Transact. Ultrasonics, Ferroelectrics & Freq. Control. 55, 2008, 2298.
[53] Alghane M, Fu Y Q, Li Y, Luo J K, Bobbili B, Feng Y, Liu Y F, Hao Z C, Chen B X, Markx G, Wang C H and Walton A J; J. Microeng. Micromech. 21, 2011, 015005.
[54] Campbell J C and Jones W R; IEEE Trans. Sonics Ultrason. 15, 1968, 209.
[55] Trujillo F J and Knoerzer K, Proc. 7th Int. Conf. CFD in minerals & Process Ind. CSIRO, Melbourne, Australia, 9, Dec. 2009.
[56] Luo J K, Fu Y Q, Li Y F, Du X Y, Flewitt A J, Walton A J, Milne W I; J. Micromech. Microeng.19, 2009, 54001.
[57] Sritharan K, Strobl C J, Schneider M F, Wixforth A and Guttenburg Z; Appl. Phys. Lett. 88, 2006, 054102.
[58] Shilton R, Tan M K, Yeo L Y and Friend J R; J. Appl. Phys.104, 2008, 014910.
[59] Nakamura H, Yamada T, Ishizaki T and Nishimura K; IEEE Trans. On Ultrasonics. Ferroelectric. Freq. Control. 49, 2004, 761.
[60] Lehtonen S, Plessky V P, Hartmann C S and Salomaa M; IEEE Trans. Ultras. Ferroelectri. Freq. Control. 51, 2004, 1697.
[61] Du X Y, Fu Y Q, Tan S C, Luo J K, Flewitt A J, Milne W I, Lee D S, Maeng S, Kim S H, Park N M, Park J and Choi Y J; Appl. Phys. Lett. 93, 2008, 094105.
[62] Toegl A, Kirchner R, Gauer C, Wixforth A; J. Biomed. Technol. 14, 2003, 197.

[63] Wixforth A, Strobl C, Gauer C, Toegl A, Sciba J, Guttenberg Z V; Anal. Biomed. Chem. 379, 2004, 982.
[64] Newton M I, Banerjee M K, Starke T K, Bowan S M, McHale G; Sensor & Actuat. 76, 1999, 89.
[65] Chono K, Shimizu N, Matsu Y, Kondoh J, Shiokawa S; Jap. J. Appl. Phys. 43, 2004, 2987.
[66] Murochim N, Sugimoto M, Matui Y, Kondoh J; Jap. J. Appl. Phys. 46, 2007, 4754.
[67] Renaudin A, Tabourier P, Zhang V, Camart J C, Druon C; Sensor & Actuat. B113, 2006, 387.
[68] Toegl A, Scribe J, Wixforth A, Strobl C, Gauer C, Guttenburg Z V; Anal. Bioanal. Chem. 379, 2004. 69.
[69] Franke T and Wixforth A; Chem Phys Chem. 9, 2008, 2140.
[70] Du X Y, Swanwick M, Fu Y Q, Luo J K, Flewitt A J, Lee D S, Maeng S, Milne W I; J. Micromech. Microeng. 19, 2009, 035016.
[71] Fu Y Q, Garcia-Gancedo L, Pang H F, Porro S, Gu Y W, Luo J K, Zu X T, Placido F, Wilson J I B, Flewitt A J and Milne W I; Biomicrofluidics, 6, 2012, 024105.
[72] Zhang A L, Wu Z Q, Xia X H; Talanta, 84, 2011, 293.
[73] Luong T D, Phan V N and Nguyen N T; Microfluidic Nanofluid.10, 2011, 619.
[74] Wixforth A; JALA, 18, 399, 2006,
[75] D.Beyssen, L.Le.Brizoual, O.Elmazria and P.Alnot; Sens. & Actuat. B118, 2006, 380.
[76] M. Alghane, Y. Q. Fu1, B. X. Chen1, Y. Li, M. P. Y. Desmulliez and A. J. Walton, Microfluid. & Nanoflud. Submitted.
[77] Du X Y, Fu Y Q, Luo J K, Flewitt A J and Milne W I; J. Appl. Phys. 105, 2009, 024508.
[78] Nguyen N T and White R T; Sens. & Actuat. 77, 1999, 229.
[79] Moroney R M, White R M, Howe R T; Appl. Phys. Lett. 59, 1991, 774.
[80] Ogawa J, Kanno I, Kotera H, Wasa K, Suzuki T; Sens. & Actuat. A52, 2009, 211.
[81] Li Y, Flynn B W, Parkes W, Liu Y, Feng Y, Ruthven A D, Terry J G, Haworth L I, Bunting A, Stevenson J T M, Smith S, Bobbili P, Fu Y Q and Walton A J; Proc. European Solid State Device Res. Conf. pp.14-18, 2009.
[82] Li Y, Fu Y Q, Brodie S, Mansuor R and Walton A, Biomicrofluid. 6, 2012, 012812.
[83] Bennès J, Alzuaga S, Ballandras S, Chérioux F, Bastien F and Manceau J F; Proc. IEEE Ultrason. Symp. Rotterdam, pp.823-826, 2005.
[84] Tan M K, Friend J R and Yeo L Y; Phys. Rev. Lett. 103, 2009, 024501.
[85] Qi A, Friend J R and Yeo L Y; Proc. 2nd Micro/nanoscale heat & mass Transf. Int Conf. Shanghai, pp.1-8, 2009.
[86] Lucklum R and Hauptmann P; Meas. Sci. Technol. 14, 2003, 1854.
[87] Grate W J, Martin S J, White R M; Anal Chem. 65, 1993, 940.
[88] Cote G L, Lec R M, Pishko M V; IEEE Sens. J. 3, 2003, 251.
[89] Kuznestsova L A and Coakley W T; Biosens. & Bioelectron. 22, 2007, 1567.
[90] Teles F R R and Fonseca L P; Talanta, 77, 2008, 606.
[91] Vellekoop M J; Ultasonics. 36, 1998, 7.
[92] Gizeli E; Smart. Mater. Struct. 6, 1997, 700.
[93] Sauerbrey G. Verwendung von Schwingquarzen zur Wagung dunner Schichten und zur Microwagang. Z. Phys. 155, 1959, 206.

[94] Nomura T, Okuhara M; Anal. Chim. Acta. 142, 1982, 281.
[95] Lin T Y, Hu C H and Chou T C; Biosens. & Bioelectron. 20, 2004, 75.
[96] Maturos T, Wong-ek K, Sangworasil M, Pintavirooj C, Wisitsora-at A and Tuantranont A; Proc. Int. Conf. Electric/Electron. Eng. Comput, Telecom. & Info Tech. Vol.1, 478, 2009.
[97] Han J H, Zhang J P, Xia Y T, Li S H and Jiang L; Colloid. & Surf. A: Physicochem. Eng. Aspects 379, 2011, 2.
[98] Dickert F L, Hayden o, Blindeus R, Mann K J, Blaas D and Waigmann E, Anal Bioanal Chem, 378, 2004, 1929.
[99] Wolfbeis O S, Editor, Springer Series on Chemical Sensors and Biosensors, Methods and applications, 2007, Volume 5, Part C, 371-424,
[100] Wang Q J, Pflugl C, Andress W F, Ham D, Capasso F and Yamanishi M; J. Vac. Sci. Technol. B26, 2008, 1848.
[101] Kirsch P, Assouar M B, Elmazria O, Mortet V and Alnot P; Appl. Phys. Lett. 88, 2006, 223504.
[102] Barie N and Rapp M; Biosensors & Bioelectron. 16, 2001, 978.
[103] Kovacs G and Venema M; Appl. Phys. Lett. 61, 1992 639.
[104] Josse F, Bender F, Cernosek R W; Anal. Chem. 73, 2001, 5937.
[105] Mchale F G; Meas. Sci. Technol, 14, 2003, 1847.
[106] Lindner G; J. Phys. D. 41, 2008, 123002.
[107] Lee D S, Lee J H, Luo J K, Fu Y Q, Milne W I, Maeng S and Jung M Y; J. Nanosci. Nanotechnol. 9, 2009, 7181.
[108] Jian S J, Chu S Y, Huang T Y and Water W; J. Vac. Sci. Technnol. A22, 2004, 2424.
[109] Krishnamoorthy S and Iliadis A A; Solid-State Electronics, 50, 2006, 1113.
[110] Mchale G, Newton M I, Martin F; J. Appl. Phys. 91, 2002 9701.
[111] Powell D A, Zadeh K K, Wlodaiski W; Sens. & Actuat. A115, 2004, 456.
[112] Du J and Harding G L ; Sens. & Actuat. A65, 1998, 152.
[113] Kao K S, Cheng C C, Chen Y C and Lee Y H; Appl. Phys. A76, 2003,1125.
[114] Kao K S, Cheng C C, Chen Y C, et al., Appl. Surf. Sci. 230, 2004, 334.
[115] Gabl R, Feucht H D, Zeininger H, Eckstein G and Wersing W; Biosens. Bioelectron. 19, 615 (2004).
[116] Lanz R and Muralt P; IEEE Trans. Utralson, Ferroelectric & Freq. Control, 52, 2005, 936.
[117] Luo J K, Ashley G M, Garcia-Gancedo L, Kirby P B, Flewitt A J and Milne W I; Int. J. Nanomanufact. 7, 2011, 448.
[118] Lin R C, Chen Y C, Chang W T, Cheng C C, Koo K S; Sens.& Actuat. A147, 2008, 425.
[119] Yan Z, Song Z, Liu W, Appl. Surf. Sci. 253, 2007, 9372.
[120] Muller A, Neculoiu D, Vasilache D, Konstantinidis G, Grenier K, Dubuc D, Bary L, Plana R and Flahaut E; Appl. Phys. Lett. 89, 2006, 143122.
[121] García-Gancedo L, Al-Naimi F, Flewitt A J, Milne W I, Ashley G M, Luo J K, Zhao X B and Lu J R; IEEE Trans Ultrason. Ferroelectric & Freq. Control. 58, 2011, 2438.
[122] García-Gancedo L, Zhu Z, Iborra E, Clement M, Olivares J, Flewitt A J, Milne W I, Ashley G M, Luo J K, Zhao X B and Lu J R; Sens. & Actuat. B160, 2011, 1386.

[123] Zhao X B, Ashley G M, Garcia-Gancedo L, Jin H, Luo J K, A J Flewitt and Lu J R; Sens. & Actuat. B163, 2012, 242.
[124] Zhang H, Marma M S, Kim E S, McKenna C E and Thompson M E; J. Micromech. Microeng. 15, 2005, 1911.
[125] Weber J, Albers W M, Tuppurainen J, Link M, Gabl R, Wersing W, Schreiter M; Sensors & Actuat. A128, 2006, 84.
[126] Link M, Webber J, Schreiter M, Wersing W, Elmazria O, Alnot P; Sensors & Actuat. B121, 2007, 372.
[127] Ho G K, Abdolv R and Ayazi F; Digest of MEMS 2007, Kobe, Japan, pp.791-795, 2007.
[128] Corso C D, Dickherber A and Hunt W D; J. Appl. Phys. 101, 2007, 054514.
[129] Ho G K, Abdolv R, Sivapurapu A, Humad S and Ayazi F; J. Microelectromech. Syst. 17, 2008, 512.
[130] Dickherber A, Corso C D and Hunt W D; Sens. & Actuat. A144, 2008, 7.
[131] Wenzel S and White R; Sens. & Actuat. A21–23, 1990, 700.
[132] White R M; Faraday Discuss. 107, 1997, 1.
[133] Huang I Y and Lee M C; Sens.& Actuat. B132, 2008, 340.
[134] Guttenberg Z, Muller H, Habermuller H, Geisbauer A, Pipper J, Felbel J, Kielpinski M, Scriba J and Wixforth A, Lab Chip. 5, 2005, 308.
[135] Raghavan R V, Friend J and Yeo L Y; Microfluid. Nanofluid. 8, 2009, 0452.
[136] Wood C D, Evens S D, Cumingham J E, O'Rorke R, Walti C and Davies A G, Appl. Phys. Lett. 92, 2008, 044104.
[137] Laurell T, Petersson F and Nilsson A; Chem. Soc. Rev. 36, 2007, 492.
[138] Shi J J, Ahmed D, Mao X L, Lin S C S, Lawit A and Huang T J; Lab Chip. 9, 2009, 2890.
[139] Wiklund M, Gunther C, Lemor R, Jager M, Fuhr G and Hertz H M; Lab Chip. 6, 2006,1537.
[140] Li H Y, Friend J R and Yeo L Y; Biomaterials, 28, 2007, 4098.
[141] Friend J R, Yeo Y L, Arifin D R and Mechler A; Nanotechnol. 19, 2008, 145301.
[142] Alvarez M, Friend J R and Yeo L Y; Langmuir, 24, 2008, 10629.
[143] Galopin E, Beaugeois M, Pinchemel B, Camart J, Bouazaoui M and Thomy V; Biosens. & Bioelectron. 23, 2007, 746.